




# Microstructure and properties of Sn-Ag and Sn-Sb lead-free solders in electronics packaging: a review

Xi Wang<sup>1</sup>, Liang Zhang<sup>1,2,\*</sup> , and Mu-lan Li<sup>1</sup>

<sup>1</sup>School of Mechatronic Engineering, Jiangsu Normal University, Xuzhou 221116, China

<sup>2</sup>State Key Laboratory of Advanced Welding and Joining, Harbin Institute of Technology, Harbin 150001, China

**Received:** 6 October 2021

**Accepted:** 18 November 2021

**Published online:**

1 December 2021

© The Author(s), under exclusive licence to Springer Science+Business Media, LLC, part of Springer Nature 2021

## ABSTRACT

Electronic devices need to work at high temperature in some fields for a long time, peculiarly step soldering technology, primary packaging and flip-chip connections, etc., along with the application of electronic products more and more widely. These phenomena promote the further development of high-temperature solders. Because of the high melting temperatures of Sn-Ag and Sn-Sb, they are suitable for high-temperature fields such as automotive electronics and avionics. In this review, the influences of trace elements and nanoparticles on microstructure, intermetallic components (IMC) growth, mechanical properties, wettability, melting behavior, and creep behavior of Sn-Ag and Sn-Sb solders have been summarized systematically. It was found that the addition of trace elements or nanoparticles into solders to be beneficial in improving the performance of Sn-Ag and Sn-Sb solders. Besides, the melting behavior of the solder at high temperatures can be further improved if Sn-Ag and Sn-Sb are used better as high-temperature solders.

## 1 Introduction

The tin-lead solders have been widely applied in electronic industry because of their good properties, for example, low melting point, great wettability, mechanical properties, and low cost [1, 2]. Nevertheless, the traditional tin-lead solders have certain toxicity, which is detrimental to human beings and ecosystem [3]. Thus, the European Union (EU) issued two directives on RoHS (Restriction of Hazardous Substances) and WEEE (Waste Electrical and Electronic Equipment), prohibiting the use of Pb in electrical devices in 2003 [4]. Sn-Pb solders progressively

took the place of lead-free solders in electronic packaging [5]. At present, the lead-free solders that have been widely used for electronic packaging are mainly Sn-Ag [6, 7], Sn-Ag-Cu [8, 9], Sn-Zn [10], Sn-Cu [11], Sn-Bi [12, 13], etc., in recent years.

With the continuous expansion in the field of electronic products, electronic devices are required to work continuously in high-temperature environments in some fields. There are many studies about lead-free solders now, but only a small part of researches are about high-temperature lead-free solders [14]. To withstand the temperature of 150–200 °C is one of the conditions to choose high-

Address correspondence to E-mail: zhangliang@jsnu.edu.cn

temperature solder [15]. Table 1 summarizes the solid temperature and liquid temperature of typical Sn-based lead-free solders. The liquid temperature of Sn-3.5Ag, Sn-5Sb, and Sn-10Sb is about 221 °C, 245 °C, and 250 °C, respectively [16]. It can be obtained from the phase diagram of binary alloys of Sn-Ag and Sn-Sb as shown in Fig. 1 [16] and Fig. 2. Thus, Sn-Ag and Sn-Sb solders meet the melting temperature conditions of high-temperature solders and are regarded to have great probabilities to replace tin-lead solders in high-temperature fields (such as automotive electronics, avionics, etc.). Due to the special conditions of the service of automotive electronics, this puts higher requirements on the solder for automotive electronics. Solders are required to have a higher melting point temperature and also higher high temperature strength, corrosion resistance, and fatigue resistance. Previous studies have shown that Sn-Ag and Sn-Sb not only have high melting points, but also have good mechanical properties at high temperatures, so these two solders were selected for review in this paper.

Sn-Ag alloys were commercialized as early as the 1970s and are widely used in the production of automotive parts because of their heat resistance and heat fatigue properties. Similarly, Sn-Sb alloys have excellent thermal fatigue resistance and can be widely used in automotive electronics. However, the disadvantages of Sn-Ag solders have insufficient fatigue resistance and low reliability, which limit the development of Sn-Ag solders in high-temperature fields [18]. It has the potential to replace Sn-Pb solder because of the superlative thermal fatigue properties and high fracture strength of Sn-5Sb [19]. Compared with other high-temperature lead-free solders for instance Au-Sn, Au-Ge, Bi-Ag, Zn-Al, etc., the liquid temperature of Sn-Sb solder is lower. Therefore, it has certain limitations in high-temperature fields. In

order to make Sn-Ag and Sn-Sb solders more general applied in the electronic packaging, many researchers improve the characteristics of Sn-Ag and Sn-Sb solders by the means of adding trace elements or nanoparticles.

In this review, the development of Sn-Ag and Sn-Sb solders and the influence of trace elements (Cu, Ag, Bi, etc.) or nanoparticles ( $\text{Al}_2\text{O}_3$ , CNTs, ZnO, etc.) on microstructures, the IMC growth, mechanical properties, wettability, melting behaviors, and creep resistance of Sn-Ag and Sn-Sb solders are evaluated. Besides, the shortcomings of the current research and the future development direction of Sn-Ag and Sn-Sb solder are summarized for providing theoretical support for future research is put forward.

## 2 Microstructure

Microstructure is one of the criteria for evaluating solders, because the microstructure of solder has a huge influence on the performance of solder [2]. Many researchers reported that adding trace elements or nanoparticles could refine the grain of solders and then enhance the performance of solder joints based on dispersion strengthening theory [18]. Thus, exploring the microstructure of solders is the basis for studying the performance of lead-free solders.

### 2.1 Sn-Ag

The microstructure of Sn-3.5Ag consists of  $\beta$ -Sn grains and network  $\text{Ag}_3\text{Sn}$  IMC. It was observed Sn matrix and  $\text{Ag}_3\text{Sn}$  IMC in microstructure of Sn-5Ag as shown in Fig. 3. The grain size of  $\text{Ag}_3\text{Sn}$  IMC increased during isothermal aging. Grain coarsening is caused by thermal activation diffusion [20].

**Table 1** The solid temperature and liquid temperature of typical Sn-based lead-free solders

Solder	Wt. %	Solidus temperature (°C)	Liquidus temperature (°C)	References
Sn-Zn	Sn-9Zn	199.6	200.8	[113]
Sn-Bi	Sn-58Bi	138	138	[87]
Sn-Ag	Sn-3.5Ag	221	221	[18]
	Sn-3Ag	221	231	[31]
Sn-Ag-Cu	Sn-3Ag-0.5Cu	217	221	[31]
	Sn-3.8Ag-0.7Cu	216	216	[114]
Sn-Cu	Sn-0.7Cu	227	227	[2]
Sn-Sb	Sn-5Sb	233	243	[94]
	Sn-10Sb	250	250	[16]

**Fig. 1** The Sn-Ag binary phase diagram[17]

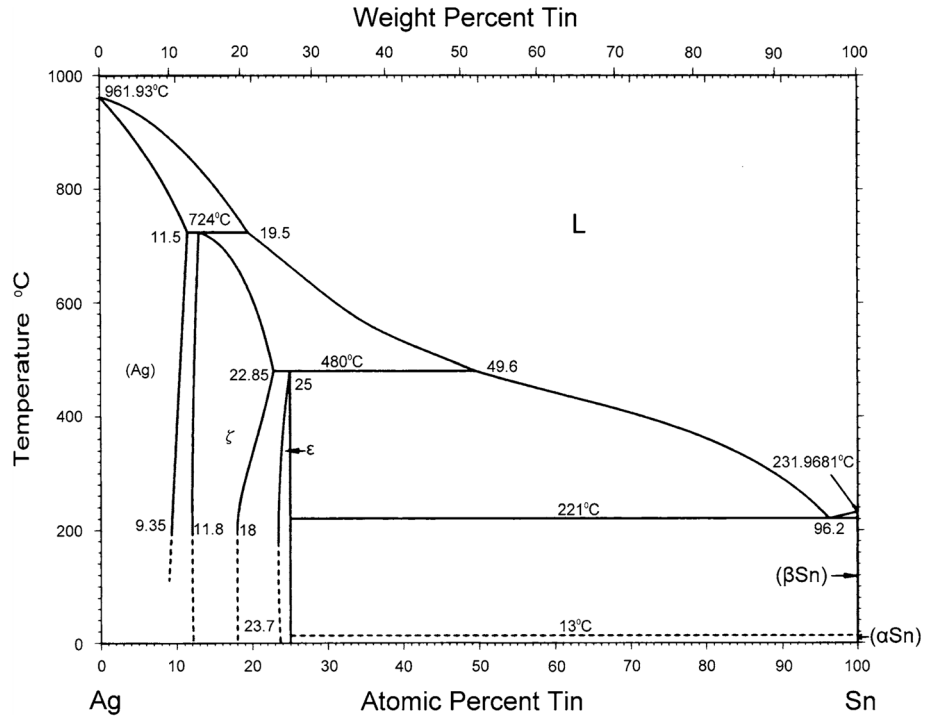
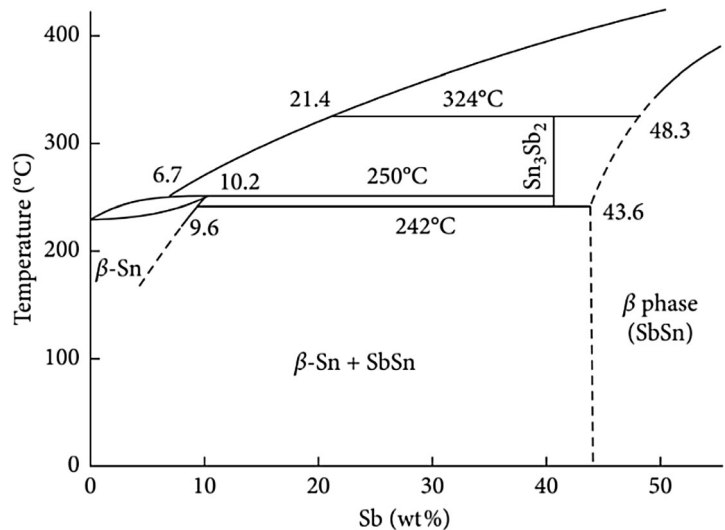


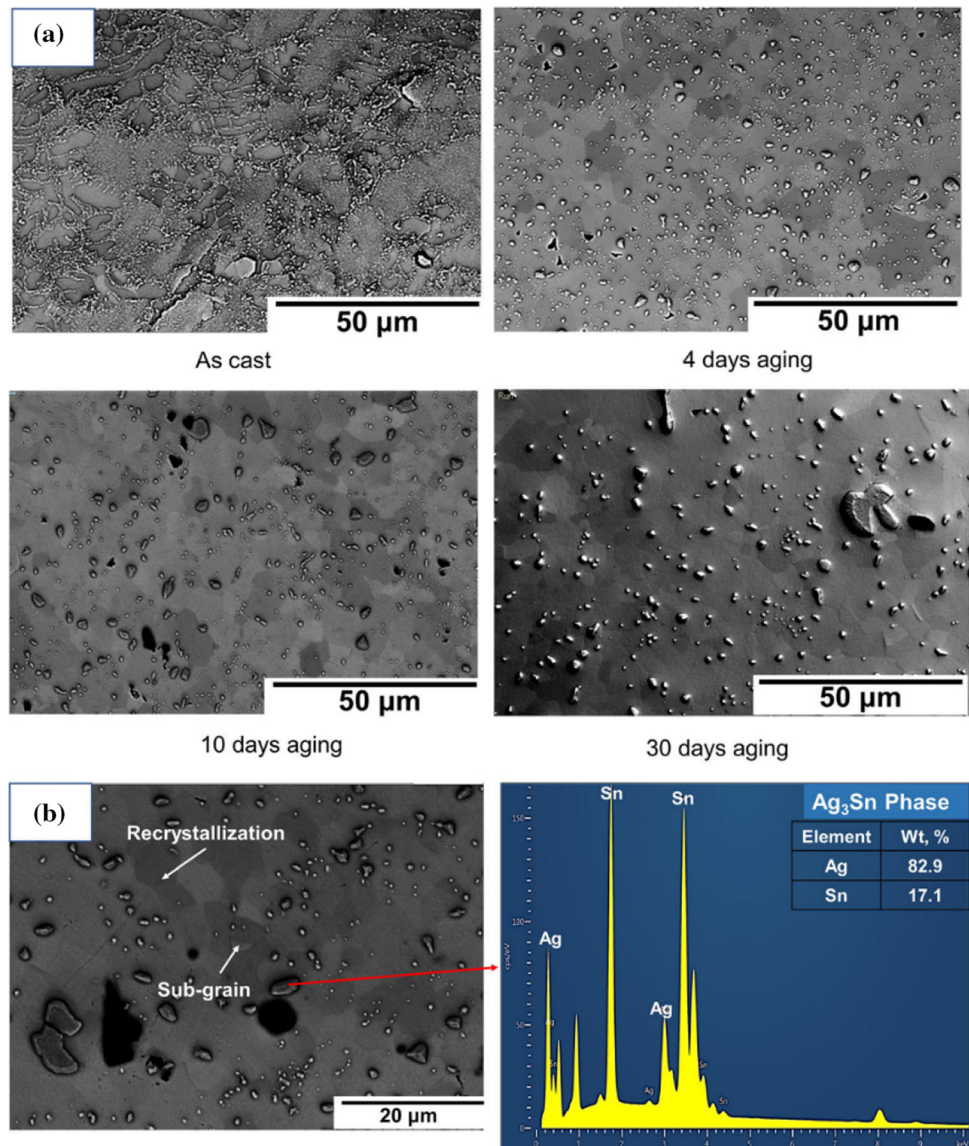
**Fig. 2** The Sn-Sb binary phase diagram[16]



On the basis of dispersion strengthening, adding trace elements or nanoparticles in solder can refine grains, thus upgrading the properties of the Sn-Ag solders. Through adding different content of Cu into the Sn-3.5Ag solder, the impact of Cu on the microstructures of solder has been probed [21]. The grains of Sn-3.5Ag-0.7Cu and Sn-3.5Ag-1.0Cu were more refined in all solders (Sn-3.5Ag, Sn-3.5Ag-0.1Cu, Sn-3.5Ag-0.3Cu, Sn-3.5Ag-0.5Cu, Sn-3.5Ag-0.7Cu, and Sn-3.5Ag-1.0Cu). Guo et al. [22] studied the microstructure of Sn-3.5Ag solder containing 15

vol% Cu or 15 vol% Ag particles during reflowing. It was found that Cu particles were almost transformed into CuSn IMC after the fourth reflow. In contrast to Sn-3.5Ag solder containing 15 vol% Cu, the AgSn IMC was not detected after four reflows in Sn-3.5Ag solder with 15 vol% Ag. Cu element diffuses faster than Ag in Sn matrix, indicating that the diffusion Sn-Cu IMC is significantly more active than the diffusion Sn-Ag IMC. Adding 1.5 wt.% Sb into Sn-3.5Ag solder can also refine grains[23]. There both are β-Sn phases and Ag<sub>3</sub>Sn IMC in Sn-3.5Ag and Sn-3.5Ag-1.5Sb, but

**Fig. 3** **a** Microstructural evolution of Sn-5Ag solder aged at 150 °C, **b** Energy dispersive x-ray spectroscopy (EDS) analysis of Sn-5Ag [20]



the size of  $Ag_3Sn$  IMC in Sn-3.5Ag-1.5Sb is smaller than Sn-3.5Ag.  $\beta$ -Sn,  $Ag_3Sn$ , and  $AgZn$  phases exist in the microstructure of Sn-3.7Ag-0.9Zn[24]. In element doping can refine  $Ag_3Sn$  and  $AgZn$  IMC in Sn-3.7Ag-0.9Zn, because In element can be adsorbed on the crystal plane to inhibit the grain growth. Peng et al. [25] researched the impact of 1.0 wt.% Al on Sn-3.7Ag-0.9Zn at high temperature. It was found that the addition of Al could also inhibit the production of  $AgZn$  and  $Ag_3Sn$  IMC and speed the production of  $Ag_2Al$  IMC in Sn-3.7Ag-0.9Zn solder. Shen et al. [26] researched the effect of nanoparticles  $ZrO_2$  on the eutectic solidification process of Sn-3.5Ag, especially on the evolution of  $Ag_3Sn$  phase. The surface energy of the crystal is reduced because of the adsorption of

$ZrO_2$ , which can significantly refine  $Ag_3Sn$  IMC. Adding 0.3 wt.% ZnO particles could also hinder the growth of  $Ag_3Sn$  and refine grains in Sn-3.5Ag, thereby enhancing the strength of solder[27].

Except the second phase strengthening, preparation method and cooling condition also affect the microstructure of the solder. Wiese et al.[28] investigated that the cooling conditions during solidification had a great influence on Sn-4Ag-0.5Cu solder. The microstructure of Sn-Ag-Cu consists of needle-shaped particles with a length of about 10 μm after slow solidification. Intermetallic spheres of sub-micron size were observed in the case of rapid solidification. Liu et al. [29] observed that the structure of the Sn-3.5Ag solder prepared by the rapid



solidification process (RSP) is more uniform and finer contrasted to Sn-3.5Ag prepared by the casting-rolling process (CRP), as shown in Fig. 4. The main reason was that RSP had a high cooling rate and large undercooling degree, which improved the role of solid solution strengthening of Ag element and made Ag element more evenly distributed in Sn matrix.

## 2.2 Sn-Sb

The grain size of Sn-5Sb solder hardly changed during the aging treatment at 150 °C [20]. The reason is that the content of Sb in the matrix increases with the raise of temperature, which enhances the influence of solid solution strengthening and inhibits the growth of grains. When the temperature increases to above 200 °C, the Sb-Sn IMC will be completely dissolved and transformed into single phase, thus promoting the growth of grains and reducing the dislocation density. Therefore, Sn-5Sb solder has relatively stable microstructure. El-Daly et al. [30] found that the size of Sb-Sn particles in Sn-5Sb was about 6 μm, only a small part of the size was about 0.6 μm uniformly distributed in the β-Sn matrix. Diverse radius of adjacent grains of the Sb-Sn IMC could make the solder diffuse into bigger grains, on the basis of Ostwald ripening mechanism, resulting in the reduction of smaller grains and the enlargement of bigger grains.

Sn-5Sb solder mainly consists of β-Sn matrix and Sb-Sn IMC. Additional phases of Ag<sub>3</sub>Sn IMC and

AuSn<sub>4</sub> IMC exist in Sn-5Sb-3.5Ag and Sn-5Sb-1.5Au solder, respectively [31]. It was observed that adding Ag and Au could refine grain in Sn-5Sb solder, and the grain of Sn-5Sb-1.5Au is smaller. El-Daly et al. [32] investigated the influence of trace elements Ag and Cu on Sn-5Sb solder. There are β-Sn, Sb-Sn, and Ag<sub>3</sub>Sn IMC in Sn-5Sb-0.7Ag, in which the morphology of β-Sn changes from equiaxed crystal to dendritic crystal with size less than 30 μm. There are β-Sn, Cu<sub>6</sub>Sn<sub>5</sub>, and Cu<sub>3</sub>Sn IMC in Sn-5Sb-0.7Cu. β-Sn grains were refined in Sn-5Sb-0.7Cu solder because of the forming of Cu<sub>6</sub>Sn<sub>5</sub> and Cu<sub>3</sub>Sn IMC, and the grain size of β-Sn grains was less than 15 μm. Therefore, adding Cu can refine the grain of solder better than Ag. Adding 1 wt.% and 2 wt.% Bi in Sn-10Sb can be completely dissolved in the matrix [33]. The addition of 3 wt.% Bi can promote the formation of Sn-Sb IMC and refine the grains of the solder. Therefore, adding 3 wt.% Bi elements in Sn-5Sb can refine the grain of solder. Geranmayeh et al. [34] added different contents of Bi and Ag in Sn-5Sb solder to form three kinds of composite solder Sn-5Sb-1.5Bi, Sn-5Sb-1.5Ag, and Sn-5Sb-1Ag-1Bi. Sn-5Sb solder is composed of β-Sn and sparse needle-like Sn-Sb particles distributed along the grain boundary, with a dendrite arm spacing of about 35 μm. The grains of Sn-5Sb-1.5Bi solder are similar to Sn-5Sb solder, and no new phase is generated. However, fine equiaxed grains with a grain size of about 4.5 μm are observed, indicating that the grains were refined. Some

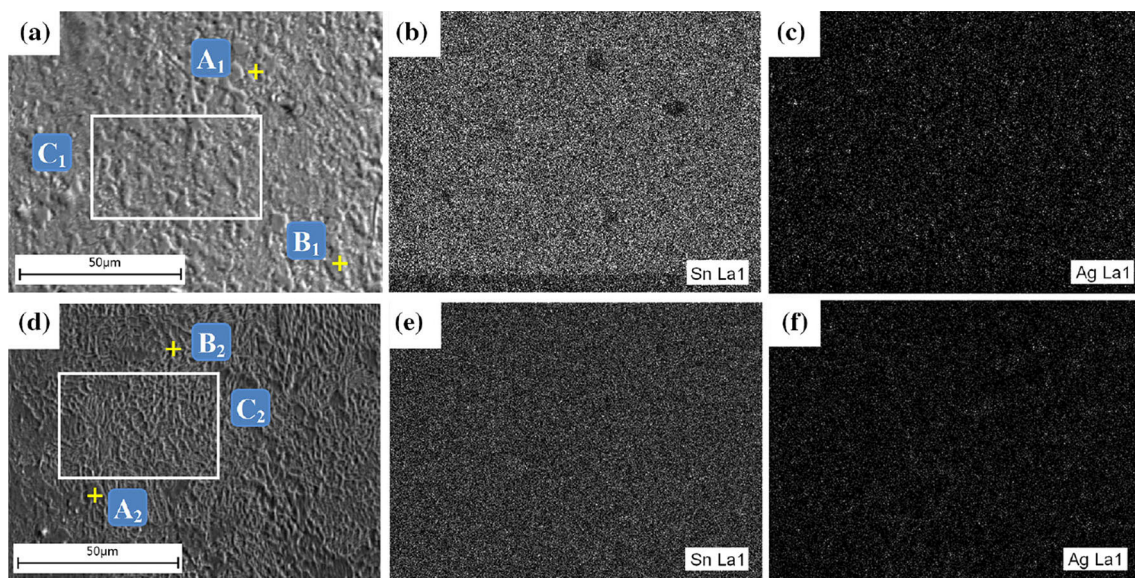


**Fig. 4** The electron probe X-ray microanalyzer (EPMA) and element distribution of Sn-3.5Ag solder: **a, b, c** CRP, **d, e, f** RSP [29]

spherical Sn-Sb IMC and columnar  $\text{Ag}_3\text{Sn}$  IMC with size of about  $15\ \mu\text{m}$  can be found in the grain boundary of Sn-5Sb-1.5Ag solder and the grain interior of the matrix. The same Sn-Sb IMC and  $\text{Ag}_3\text{Sn}$  IMC were also found in Sn-5Sb-1Ag-1Bi solder. The addition of 2 wt.% In element in Sn-10Sb solder can form a new tetragonal  $\text{In}_3\text{Sn}$  phase with a size of about 66.5 nm and can also refine the  $\beta$ -Sn and Sb-Sn phase [35]. The grain size of  $\beta$ -Sn phase decreases from 182.8 nm to 56.5 nm, and the grain size of Sb-Sn phase decreases from 160.5 nm to 60.3 nm.

In addition to alloying elements, many researchers found that adding nanoparticles could also improve the microstructure of the solder. Adding 0.3wt.% ZnO nanoparticles can refine  $\text{Ag}_3\text{Sn}$  and Sn-Sb particles in Sn-5Sb-1.5Ag (SSA) solder, mainly because of the powerful adsorption and high surface free energy of ZnO nanoparticles [36]. Because of the diffusion-controlled Ostwald ripening mechanism, large precipitates continue to grow and small precipitates shrink, resulting in grain coarsening after aging treatment. Mansour et al. [37] also found that the addition of 0.3wt.% ZnO particles could refine the grain sizes of Sn-Sb,  $\text{Ag}_3\text{Sn}$ , and  $\beta$ -Sn in Sn-5Sb-1.5Ag solder. The addition of 0.2 wt.% graphene oxide nanosheets (GONSs) to Sn-5Sb-1Ag solder can hinder the growth of IMC and refine  $\text{Ag}_3\text{Sn}$  and Sn-Sb IMC [38]. Because of the adsorption of GONSs, the interface energy between IMC and GONSs increases. The thermodynamic resistance of IMC grain growth is proportional to interfacial energy, thereby inhibiting the surface diffusion of IMC. This process is the reason why IMC grains become smaller. In addition, Eid et al. [39] studied the effect of heat treatment at  $130\ ^\circ\text{C}$  for 2 h at high pressure (1.0 GPa) on Sn-5Sb-0.3Cu (SSC-503) solder. It was discovered that the microstructure of SSC-503 solder was irregular wavy coarse grains. At  $130\ ^\circ\text{C}$ , the grains of SSC-503 solder were refined after 2 h treatment (SSC-HT), and the IMC of  $\text{Cu}_6\text{Sn}_5$  decreases from about  $26\ \mu\text{m}$  to about  $12\ \mu\text{m}$ . The SSC-503 solder was subjected to heat treatment and pressure of 1.0 GPa (SSC-PHT). As shown in the Fig. 5, a part of the  $\text{Cu}_6\text{Sn}_5$  IMC was broken, and the applied pressure caused large lattice strain and the crystal defect, thereby improving mutual solubility of the solder. Many dislocations are generated in the crystal due to the application of pressure, resulting in the increase of lattice strain and the decrease of grain size. Dias et al. [40] found that the microstructure of Sn-10Sb solder was honeycomb

$\beta$ -Sn and  $\text{Sn}_3\text{Sb}_2$  IMC in the cooling range of 2.5–25 K/s, and the gains spacing increased with the decrease of cooling rate.

Table 2 recaps the influence of trace element on the microstructure of Sn-Ag and Sn-Sb solder. Table 2 displays that adding trace elements or nanoparticles could refine the grain of solder and produce new phase. Moreover, the grains can be refined by changing cooling condition of solder. On the basis of the fine grain strengthening, solders with refined microstructure have higher strength, hardness, plasticity, and toughness at room temperature. Therefore, many researchers advance the mechanical properties of solder by improving the microstructure of solder.

### 3 Interfacial IMC growth

Reliability of solder joints is closely related to the evolution of IMC, and the diffusion of elements is the key to interfacial reaction [41]. The schematic diagram of interface microstructure of two solder joints is shown in Fig. 6. Adding trace elements or nanoparticles will affect the diffusion of elements, thereby improving the performance of solder joints [18].

#### 3.1 Sn-Ag

The reaction of Sn with Ni substrate will form microvoids. Yu et al. [42] found that adding Ag element could inhibit the formation of microvoids. When the content of Ag is less than 2.4 wt.%, there

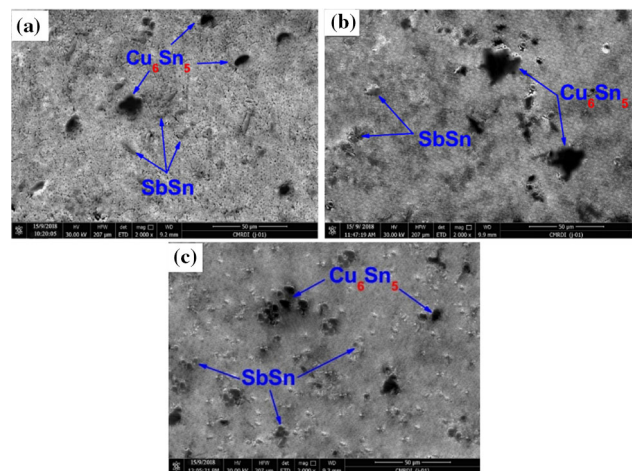


**Fig. 5** Microstructure of **a** SSC-503, **b** SSC-HT, and **c** SSC-PHT [39]

**Table 2** Effect of trace element on the microstructure of Sn-Ag and Sn-Sb solder

Solder	Element	Wt.%	Grina Size	New phase	References
Sn-Ag	Cu	0.1–1.0	↓	Cu <sub>6</sub> Sn <sub>5</sub>	[21]
	Sb	1.5	↓	Sn-Sb	[23]
	Zn, In	0.9,0.5/1.0	↓(5 μm/3 μm)	AgZn	[24]
	Al	1.0	↓(20 μm)	Ag <sub>2</sub> Al	[25]
	ZrO <sub>2</sub> nanoparticles	2	↓↓		[26]
	ZnO nanoparticles	0.3	↓		[27]
Sn-Sb	Ag	3.5	↓	Ag <sub>3</sub> Sn	[31]
	Au	1.5	↓↓	AuSn <sub>4</sub>	[31]
	Ag	0.7	↓(< 30 μm)	Ag <sub>3</sub> Sn	[32]
	Cu	0.7	↓↓(< 15 μm)	Cu <sub>6</sub> Sn <sub>5</sub> , Cu <sub>3</sub> Sn	[32]
	Bi	3	↓		[33]
	Ag	1.5	↓(15 μm)	Ag <sub>3</sub> Sn	[33]
	Bi	1.5	↓↓(4.5 μm)		[33]
	Ag, Bi	1.0, 1.0	↓↓		[33]
	In	2.0	↓↓(60 nm)		[35]
	Ag,	1.5,0.3	↓	Ag <sub>3</sub> Sn	[37]
	ZnO nanoparticles				
	Ag, GONSs	1.5,0.2	↓	Ag <sub>3</sub> Sn	[38]
	Cu	0.3	↓		[39]

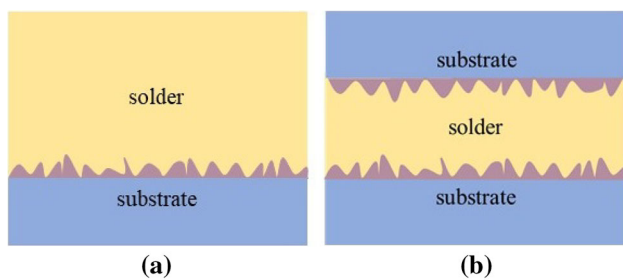


**Fig. 6** The schematic diagram of interfacial microstructure in **a** two-dimensional and **b** sandwich-structure solder joints

still are voids in the interface. When the content of Ag is more than 3.5 wt.% and less than 8.0 wt.%, large Ag<sub>3</sub>Sn forms in the interface. However, Ag content has small effect on the evolution of Ni<sub>3</sub>Sn<sub>4</sub> IMC. Therefore, the optimal addition of Ag is 2.4–3.5 wt.%. Guo et al. [43] found that there were fan-shaped Cu<sub>6</sub>Sn<sub>5</sub> IMC at the interface of Sn-3.5Ag/Cu, as shown in Fig. 7, and the IMC particles were refined but the height of IMC layers increases, compared with Sn/Cu solder joints. Besides Ag<sub>3</sub>Sn IMC distributed on the boundary rather than on the top at the heat preservation stage. The Ag<sub>3</sub>Sn IMC can inhibit the evolution of Cu<sub>6</sub>Sn<sub>5</sub> IMC in Sn-3.5Ag/Cu [44]. Unlike Sn/Cu interface, Ag<sub>3</sub>Sn IMC adsorbed on Cu<sub>6</sub>Sn<sub>5</sub> IMC is formed at Sn-3.5Ag/Cu interface, as shown in Fig. 8. The Ag<sub>3</sub>Sn is adsorbed on Cu<sub>6</sub>Sn<sub>5</sub> IMC during reflow soldering, thereby reducing its

surface energy and inhibiting its growth. Therefore, Sn-Ag solder has better weldability than pure Sn solder. Yu et al. [45] studied the evolution of Cu<sub>3</sub>Sn IMC in Sn/Cu, Sn-0.7Cu/Cu, and Sn-3.5Ag/Cu solder joints under isothermal aging at 150 °C and 180 °C. It was found that Cu and Ag element could hinder the evolution of Cu<sub>3</sub>Sn IMC. It was found that the growth of Cu<sub>3</sub>Sn IMC was achieved by consuming Cu<sub>6</sub>Sn<sub>5</sub> IMC in the process of isothermal aging of Sn-3.5Ag/Cu solder joints.

The Ni<sub>3</sub>Sn<sub>4</sub> IMC, which grew parabolically during high-temperature aging, was generated in Sn-3.5Ag/Ni-plated Cu solder joint [46]. The growth of Ni<sub>3</sub>Sn<sub>4</sub> IMC showed a bulk diffusion growth mechanism when the aging temperature was close to the melting temperature of Sn-3.5Ag solder. It was found that the Ni<sub>3</sub>Sn<sub>4</sub> IMC was formed in Cu/electroless Ni-P/Sn-3.5Ag solder joints during aging, and the electroless Ni-P layer was transformed into Ni<sub>3</sub>P IMC [47]. When the electroless Ni-P layer is completely consumed, Ni<sub>2</sub>SnP compounds start to grow between Ni<sub>3</sub>Sn<sub>4</sub> and Ni<sub>3</sub>P layers. Yoon et al. [48] studied the interfacial reaction of Sn-1Ag solder with two substrates, electroless nickel-immersion gold (ENIG) and electroless nickel-electroless palladium-immersion gold (ENEPIG) substrates. The Ni<sub>3</sub>Sn<sub>4</sub> IMC was formed at the interface of Sn-1Ag/ENIG. The spallation of Ni<sub>4</sub>Sn<sub>3</sub> IMC from the interface was observed



**Fig. 7** The SEM images of **a**, **c** the top-view morphologies of the IMC grains at Sn/Cu and Sn-3.5Ag/Cu interfaces and **b**, **d** the cross-sectional of the IMC grains at Sn/Cu and Sn-3.5Ag/Cu interfaces [43]

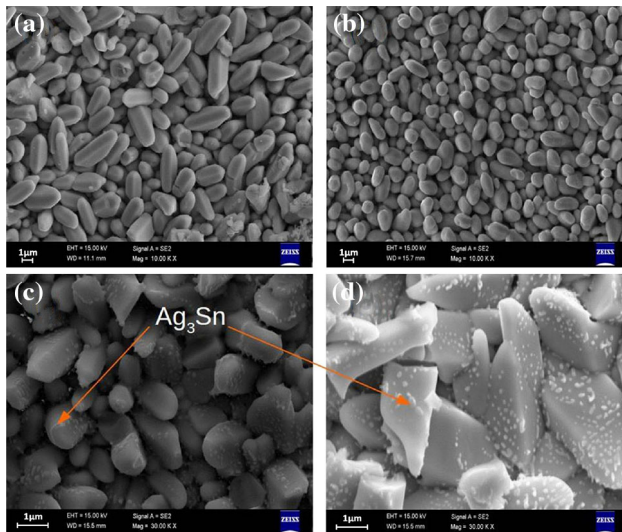
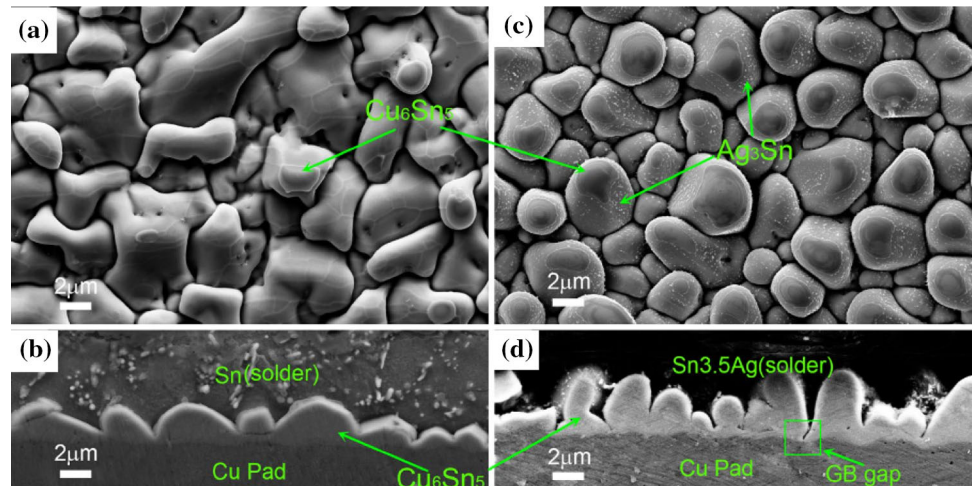


**Fig. 8** Images of the top-view of  $\text{Cu}_6\text{Sn}_5$  IMC for **a**, **b** Sn and **c**, **d** Sn-3.5Ag solders subjected to air cooling from a reflow temperature of 250 °C [44]

in Sn-1Ag/ENEPIG, and  $\text{Ni}_2\text{SnP}$  and P-rich Ni layers were formed at the interface of Sn-1Ag/Ni(P) solder joint. Sn-1Ag/ENIG solder joint has relatively good interfacial stability and limited IMC thickness, as shown in Fig. 9. During the process of reflow, the formation of stable IMC can effectively ensure the sequential solder reaction between solder and substrate.

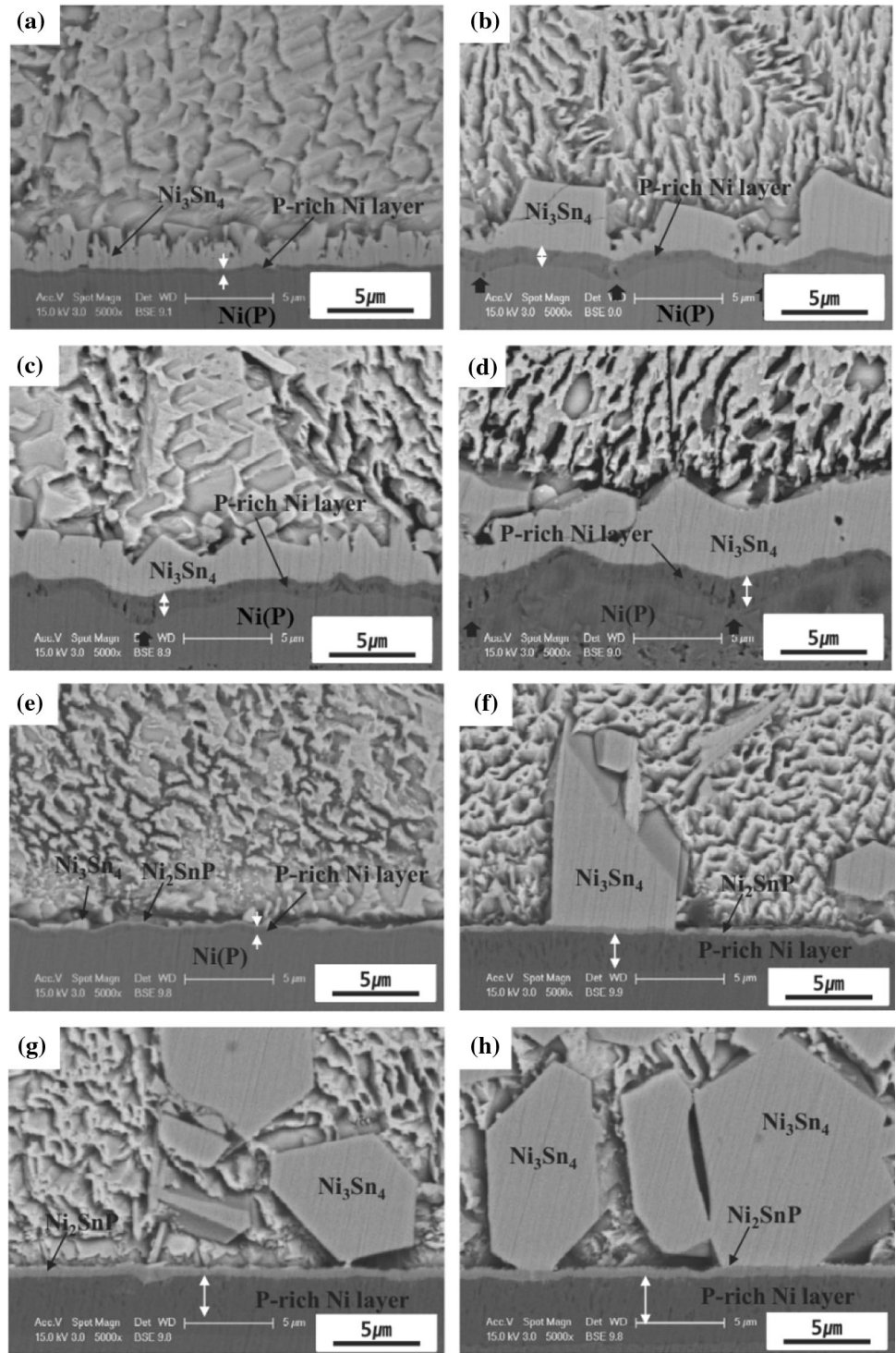
It was found that  $\gamma\text{-Ag}_2\text{Al}$  and  $\mu\text{-Ag}_3\text{Al}$  IMC were formed on Sn-3.5Ag/Al solder joint.[49]. During the aging process, the thickness of IMC layers decreases, and a part of  $\mu\text{-Ag}_3\text{Al}$  IMC transforms into  $\gamma\text{-Ag}_2\text{Al}$  IMC. Yao et al.[50] studied the microstructure and evolution of interface IMC in Sn-3.5Ag/Al solder

joint at 250 °C–285 °C for 60 min. It was found a layer of  $\text{Ag}_2\text{Al}$  IMC which contained many grains, as shown in Fig. 10. It was observed that these grains had deep gaps, and the thickness of IMC was approximately equal to the grain size. With the reflowing time increase, the thickness of IMC layer grows linearly, and then grows parabolically. These two growth conditions correspond to the chemical reaction-limited stage and the grain boundary diffusion-controlled stage, respectively. The activation energy ( $Q$ ) was  $84.105 \pm 2.571$  kJ/mol, and the grain boundary diffusion-controlled stage was  $26.385 \pm 3.171$  kJ/mol in the chemical reaction-limited stage.

Cu substrate is generally used in electronic packaging because of its great solderability and excellent thermal conductivity [51]. Kunwar et al. [52] researched the intermetallic compound growth of Cu/Sn/Cu and Cu/Sn-3.5Ag/Cu at the cold end. The IMC thickness at the cold end of Cu/Sn/Cu and Cu/Sn-3.5Ag/Cu is 36.9  $\mu\text{m}$  and 32.5  $\mu\text{m}$  at the heating plate temperature at 350 °C for 50 min, respectively. The thickness of  $\text{Cu}_6\text{Sn}_5$  IMC in Cu/Sn-3.5Ag/Cu is smaller than Cu/Sn/Cu at the cold end, because  $\text{Ag}_3\text{Sn}$  IMC can hinder the growth of  $\text{Cu}_6\text{Sn}_5$  IMC. The  $\text{Cu}_6\text{Sn}_5$  IMC was first formed at Cu/Sn-2.3Ag/Cu interface and then transformed into  $\text{Cu}_3\text{Sn}$ , because  $\text{Cu}_6\text{Sn}_5$  could not reach equilibrium with Cu [53]. Compared with the layer type of  $\text{Cu}_3\text{Sn}$ , the porous type of  $\text{Cu}_3\text{Sn}$  IMC has a larger specific surface area and higher surface energy, thus the layered structure could be formed firstly. However, the growth of porous  $\text{Cu}_3\text{Sn}$  will occur, when  $\text{Cu}_6\text{Sn}_5$  IMC cannot transform fast enough through the



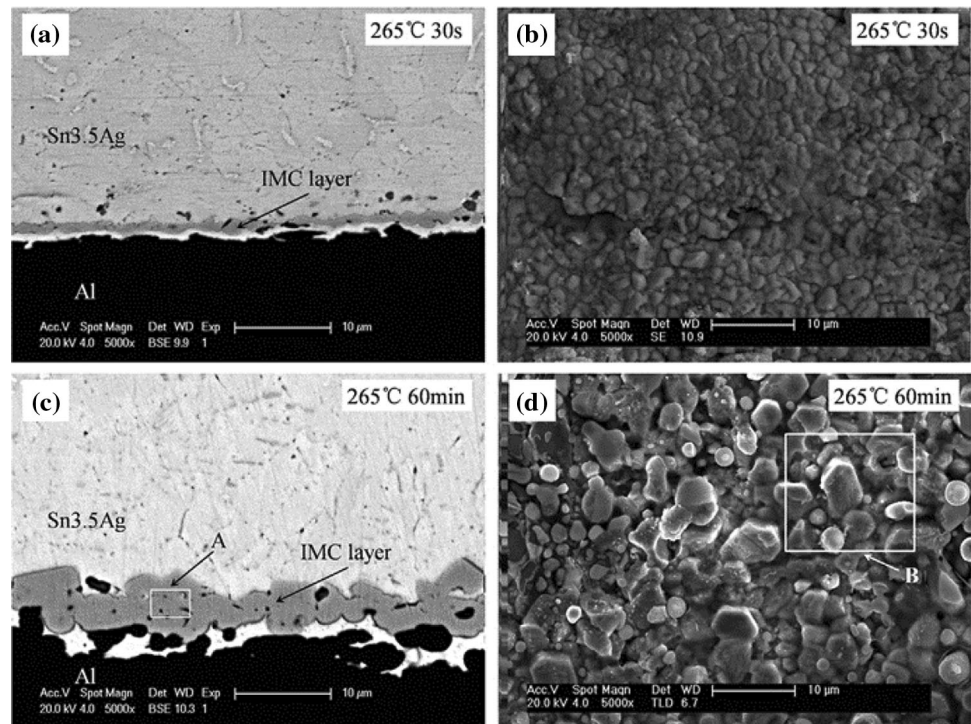
**Fig. 9** The cross-sectional SEM images of the **a, b, c, d** Sn–1Ag/ENIG and **e, f, g, h** Sn–1Ag/ENEPIG interfaces reflowed at 260 °C for different reflow times: **a, e** 1, **b, f** 10, **c, g** 30 and **d, h** 60 min [48]



growth of layered  $Cu_3Sn$ . It is found that Cu element is the main diffusion material in the layer type of  $Cu_3Sn$  IMC, while Sn is the main diffusion material in the porous type of  $Cu_3Sn$  IMC.  $Cu_3Sn$  IMC will cause large volume shrinkage, leading to many new and reliable problems, so it is very significant to research

how to inhibit the growth of  $Cu_3Sn$ . Ouyang et al. [54] studied the interfacial reaction of  $Ag_3Sn$  IMC in Ag/Sn-3.5Ag/Ag under a temperature gradient of 168.9 °C/cm at 260 °C on a hot plate. It was found that the evolution of  $Ag_3Sn$  IMC at the two plates was asymmetric, as shown in Fig. 11, during

**Fig. 10** The images of Sn-3.5Ag/Al interfaces at 265 °C: for **a** 30 s of cross section and **b** vertical section, **c** 60 min of cross section and **d** vertical section [50]



reflowing on a hot plate at 260 °C. The asymmetric growth of  $\text{Ag}_3\text{Sn}$  IMC under the temperature gradient is because of the diffusion of Ag elements from the hot end to the cold end, thereby causing the abnormal growth of  $\text{Ag}_3\text{Sn}$  IMC at the cold end.

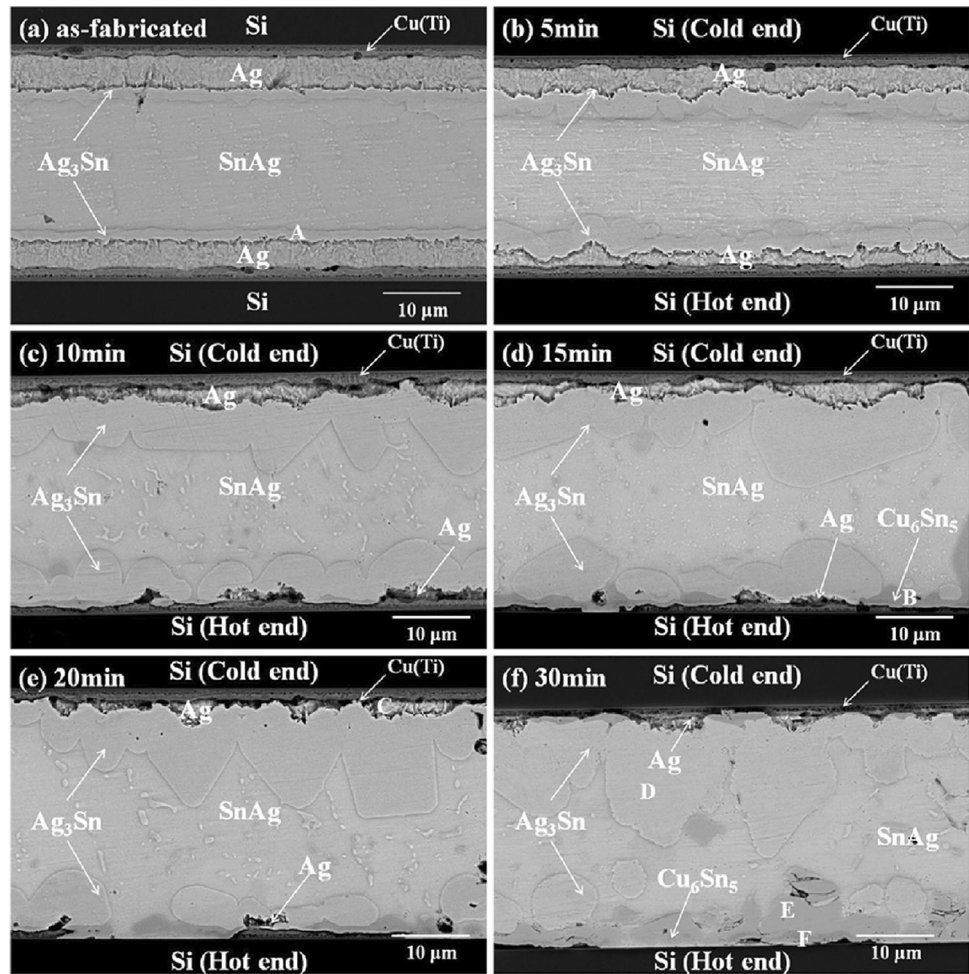
It was found that the growth rate of  $\text{CoSn}_3$  IMC at the hot end was higher than the cold end in  $\text{Co/Sn-3.5Ag/Co}$ , and Sn atom moves from the cold end to the hot end at the temperature gradient of 1644 °C/cm, which is the main diffusion material [55]. The growth rate of  $\text{Cu}_6\text{Sn}_5$  and  $\text{Cu}_3\text{Sn}$  IMC in the cold end is faster than the hot end in  $\text{Cu/Sn-3.5Ag/Co}$ , at the temperature gradient of 3868 °C/cm. It was found that Cu was the main diffusion material in  $\text{Cu/Sn-3.5Ag/Co}$  structure. In addition, Co element is not observed near the Cu substrate of  $\text{Cu/Sn-3.5Ag/Co}$  and  $\text{Co/Sn-3.5Ag/Cu}$  under the temperature gradient of 3868 °C/cm and 3136 °C/cm, as shown in Fig. 12, indicating that Co has better thermal migration resistance than Cu and Sn. Yang et al. [56] studied the growth of  $\text{Ni}_3\text{Sn}_4$  IMC in  $\text{Ni/Sn-3.5Ag/Ni}$  under a temperature gradient of 160 °C/cm at 260 °C on a hot plate. It was found that the evolution of  $\text{Ni}_3\text{Sn}_4$  IMC was divided into two stages under a temperature gradient. The evolution of  $\text{Ni}_3\text{Sn}_4$  IMC was controlled by the chemical potential gradient in stage I (0–120 min), resulting in the increase of the

thickness of  $\text{Ni}_3\text{Sn}_4$  at the hot and cold end. However, under the action of thermal migration, the growth of  $\text{Ni}_3\text{Sn}_4$  IMC is faster than the hot end. The chemical potential gradient and temperature gradient reached a dynamic equilibrium at the hot end at stage II (120–210 min), therefore the IMC thickness no longer increased with the increase of reflow time at the hot end. The evolution of IMC in  $\text{Ni/Sn-2.3Ag/Cu}$  solder joints largely depends on the thickness of the solder [57]. Contrary to Ni side, the thickness of the IMC increases as the thickness of the solder decreases on the Cu side while the time of reflowing is fixed. Besides, the concentration of Cu and Ni in the solder rises as the thickness of the solder decreases.

Many researchers have found that adding trace elements into Sn-Ag solder could advance the reliability of solder joints. Wang et al. [58] studied the reaction of Sn-2.5Ag solder with different content of Ni (0–0.1 wt.%) and two Cu substrates (electroplated Cu substrate and high-purity Cu substrate). It was found the formation of Kirkendall voids on electroplated Cu substrate, but voids were not observed when the solder reacted with high-purity Cu substrate. In addition to Kirkendall voids, the thickness and the structure of IMC formed on the two Cu substrates are similar. Adding Ni into Sn-2.5Ag solder can effectively inhibit the growth of  $\text{Cu}_3\text{Sn}$  IMC,



**Fig. 11** The cross-sectional images of Ag/Sn-Ag/Ag **a** as-fabricated, and reflowing on the hot plate at 260 °C for **b** 5, **c** 10, **d** 15, **e** 20 and **f** 30 min [54]



thereby reducing Kirkendall voids formed. Sn-3.5Ag/Cu can dissolve more Cu at higher reflow temperature [6]. It was found that adding 0.5 wt.% Cu in solder could reduce the dissolution rate of Cu. Because the concentration gradient of Cu in Sn-3.5Ag-0.5Cu solder is not high, the Cu element in Cu substrate is not easy to dissolve by solder, which makes the interface IMC more stable. As shown in Fig. 13a and b, Sn-3.5Ag and Sn-4Ag-0.5Cu have similar microstructure [59], but some  $\text{Cu}_6\text{Sn}_5$  IMC was found in Sn-4Ag-0.5Cu solder, which is larger than  $\text{Ag}_3\text{Sn}$  IMC. A new Cu-Ni-Sn IMC was formed in Sn-2.5Ag-0.5Cu-0.5Ni and Sn-2Ag-1Cu-1Ni solders, as shown in Fig. 13c and d. It was found that a small amount of  $\text{Ag}_3\text{Sn}$  IMC was present in these solders. Therefore, adding Cu and Ni element could inhibit the growth of  $\text{Ag}_3\text{Sn}$  IMC. The  $\beta$ -Sn dendrite and network  $\text{Ag}_3\text{Sn}$  phase were formed in microstructure of Cu/Sn-3.5Ag/Ni solder joint [60]. As shown in Fig. 14, the  $\beta$ -Sn dendrite, network  $\text{Ag}_3\text{Sn}$  IMC, and

(Cu, Ni) $_6\text{Sn}_5$  IMC were formed in the Cu/Sn-3.0Ag-0.5Cu/Ni solder joint. The volume fraction of  $\text{Ag}_3\text{Sn}$  in Cu/Sn-3.5Ag/Ni solder joint is higher than that in Cu/Sn-3.0Ag-0.5Cu/Ni solder joint because the content of Ag in Sn-Ag solder (3.5 wt%) is higher than that in Sn-Ag-Cu solder (3.0 wt%).

Guo et al. [22] added 15 vol% Cu and Ag particles into Sn-3.5Ag solder to research the influence of multiple reflow soldering on the interface IMC. After the first reflow, the IMC thickness of Cu-containing composite solder is 1.9  $\mu\text{m}$ , and after four reflows, the IMC thickness increases to 5  $\mu\text{m}$ . For Ag-containing composite solder, the initial IMC thickness is 1.2  $\mu\text{m}$ , and after four reflows, the IMC thickness increases to 2.8  $\mu\text{m}$ . It can be observed that adding Ag can better hinder the growth of IMC, because Ag particles can enhance the activation energy of  $\text{Cu}_6\text{Sn}_5$  phase, so that the grain nucleation is more difficult, thus inhibiting the formation of  $\text{Cu}_6\text{Sn}_5$  IMC. Adding 0.5 wt.% Zn into the Sn-3.5Ag solder has no obvious



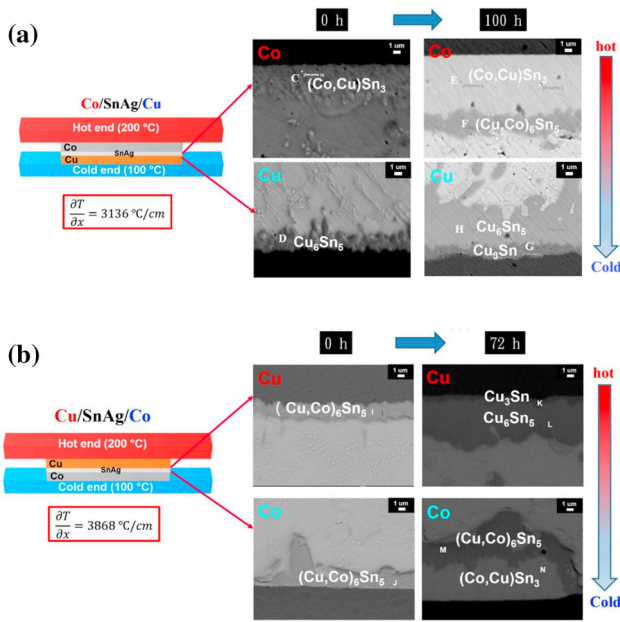


**Fig. 12** Enlarged images on evolution of IMC at the cold and the hot plates before and after thermomigration test of **a** 100 h for Co/Sn-Ag/Cu and **b** 72 h for Cu/Sn-Ag/Co [55]

inhibition effect on  $\text{Cu}_6\text{Sn}_5$  IMC, but adding 1.0 wt.% and 1.5 wt.% Zn can inhibit the growth of  $\text{Cu}_6\text{Sn}_5$  IMC and  $\text{Cu}_3\text{Sn}$  IMC, as shown in Fig. 15 [61]. The main

reason is that the Cu–Zn compound is formed during the solder reacts with the Cu substrate, which will promote the diffusion of Sn, thereby inhibiting the growth of  $\text{Cu}_6\text{Sn}_5$  IMC and  $\text{Cu}_3\text{Sn}$  IMC. Similarly, Lu et al. [62] found that the rapid reaction of Zn in Sn-10Ag-0.6Zn solder and Cu element effectively inhibited the migration of Cu. Adding 0.6 wt.% Zn in Sn-10Ag solder can improve the stability of  $\text{Ag}_3\text{Sn}$  and  $\text{Cu}_6\text{Sn}_5$  IMC in Sn-10Ag/Cu and inhibit the growth of  $\text{Cu}_3\text{Sn}$  IMC.

Besides adding trace elements, nanoparticles could also advance the reliability of solder joints. Tikale et al. [63] found that the morphology of  $\text{Cu}_6\text{Sn}_5$  IMC in Sn-3.6Ag solder is scallop-shaped. Adding 0.05 wt.% nano- $\text{Al}_2\text{O}_3$  particles to Sn-3.6Ag solder will inhibit the growth of  $\text{Cu}_6\text{Sn}_5$  IMC, mainly because nano- $\text{Al}_2\text{O}_3$  can be adsorbed on the surface of IMC, thereby reducing the diffusion of Sn. Adding 0.05 wt.% nano- $\text{Al}_2\text{O}_3$  to the solder can also refine the plate-shaped  $\text{Ag}_3\text{Sn}$  IMC in the matrix into fine spherical  $\text{Ag}_3\text{Sn}$  IMC. The uniform distribution of nano- $\text{Al}_2\text{O}_3$  and the fine spherical  $\text{Ag}_3\text{Sn}$  IMC plays the role of the second particle strengthening, thereby improving the reliability of the solder joint. Adding 0.5 wt.% ZnO particles or 0.1 wt.% or 0.3 wt.% Ge to

**Fig. 13** SEM images of samples without etching [59]

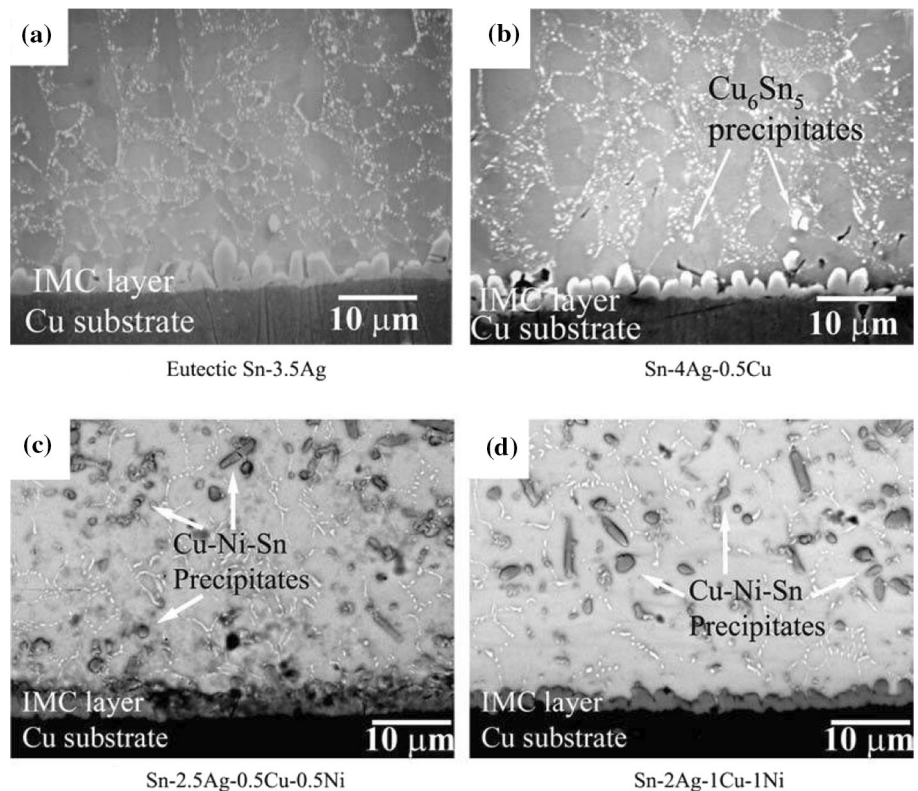
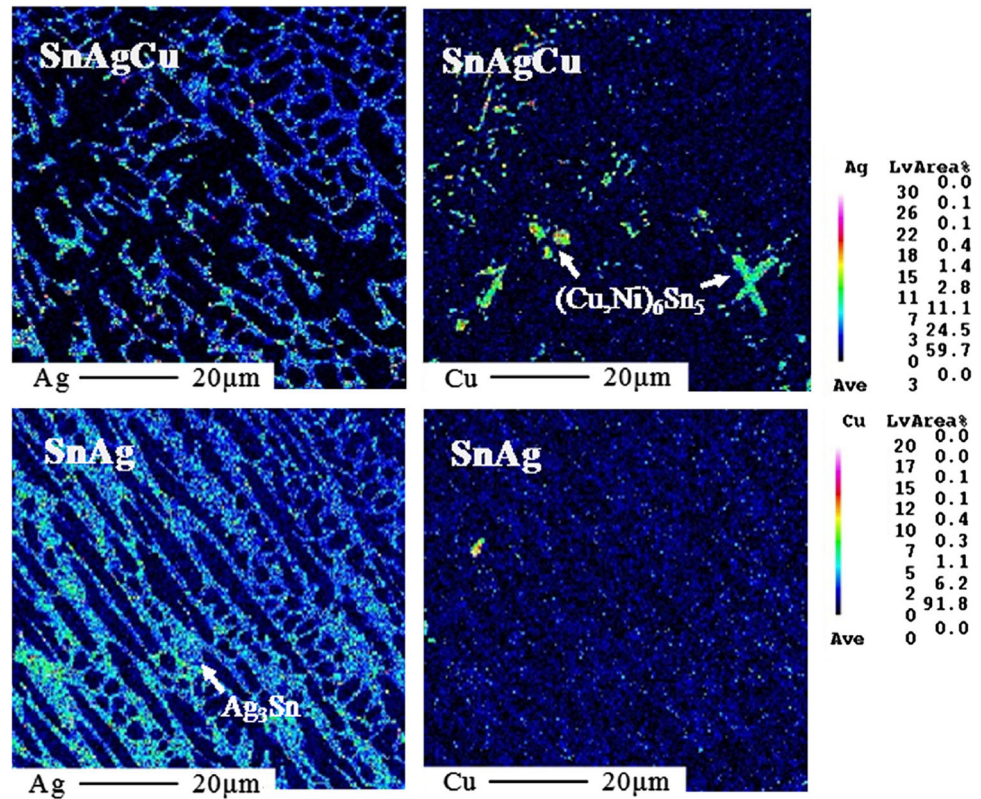


**Fig. 14** Elemental color mappings of Sn-3.0Ag-0.5Cu and Sn-3.5Ag solder joints [60]



Sn-3.5Ag solder could also hinder the evolution of  $\text{Cu}_3\text{Sn}$  IMC was investigated by Yu et al. [64].

### 3.2 Sn-Sb

At 260 °C,  $\text{Cu}_6\text{Sn}_5$  and  $\delta$  phases (the  $\delta$  phase was the mutually soluble region of  $\text{Cu}_3\text{Sn}$  and  $\text{Cu}_4\text{Sb}$ ) formed in the Sn-3Sb/Cu, Sn-5Sb/Cu, and Sn-7Sb/Cu solder joints, and the Sb content had no significant influence on the growth rate of IMC layer [65]. Tatsuya et al. [16] analyzed Sn-5Sb/Cu and Sn-10Sb/Cu solder joints by EPMA, respectively. Sn and Cu existed in Sn-5Sb/Cu solder joints, as shown in Fig. 16, while Sn-Cu and Sb-Sn compounds were observed in Sn-10Sb/Cu solder joints.  $\text{Cu}_3\text{Sn}$  IMC and  $\text{Cu}_6\text{Sn}_5$  IMC were found in both solder joints. Researchers conducted power cycling tests on the two solder joints and found that Sn-10Sb/Cu solder joints had higher reliability.  $\text{Ni}_3\text{Sn}_4$  IMC was formed in Sn-5.5Sb/Ni solder joints and  $\text{Cu}_6\text{Sn}_5$  IMC was formed in Sn-5.5Sn/Cu solder joints [66]. During solidification, Ni and Cu elements diffuse into Sn-5.5Sb solder. However, the  $\text{Cu}_6\text{Sn}_5$  IMC layer permitted a higher intensity of dissolution with respect to the molten solder. In contrast, the IMC layer was not found at the

interface between Sn-5.5Sb solder and the steel substrate. Du et al. [67] studied the electromigration effect of Cu/Sn-10Sb/Cu lead-free solder joints at 115 °C and 140 °C at  $5.0 \times 10^4$  A/cm<sup>2</sup>. The  $\text{Cu}_6\text{Sn}_5$  IMC grows at the interface anode and has a parabolic relationship with time, while it is inhibited at the cathode. While the thickness of cathode  $\text{Sn}_3\text{Sb}_2$  IMC increased, the large particles of  $\text{Sn}_3\text{Sb}_2$  IMC were formed in anode  $\text{Cu}_6\text{Sn}_5$  IMC at 140 °C. The polarity effect of IMC on the interface is mainly because of the anodic migration of Cu and Sn under the action of chemical electron wind, potential gradient, and back stress. The migration of Sb to the cathode under the back stress induced by electromigration leads to the change of IMC in  $\text{Sn}_3\text{Sb}_2$ . SnTe-Sn layer was formed at the interface of Sn-Sb/Te. Lee et al. [68] found that the growth rate of SnTe-Sn layer increased apparently with increasing Sb content in Sn-Sb/Te solder joints because Sn-Sb IMC promoted the nucleation rate of SnTe. In addition, the thickness and reaction time of SnTe-Sn layer follow parabolic law.

Adding trace elements or nanoparticles can further improve the solder joint performance. Han et al. [69] studied the microstructure evolution of IMC in Au/Sn-5Sb-1Cu-0.1Ni-0.1Ag/(Au)Ni solder joints. There

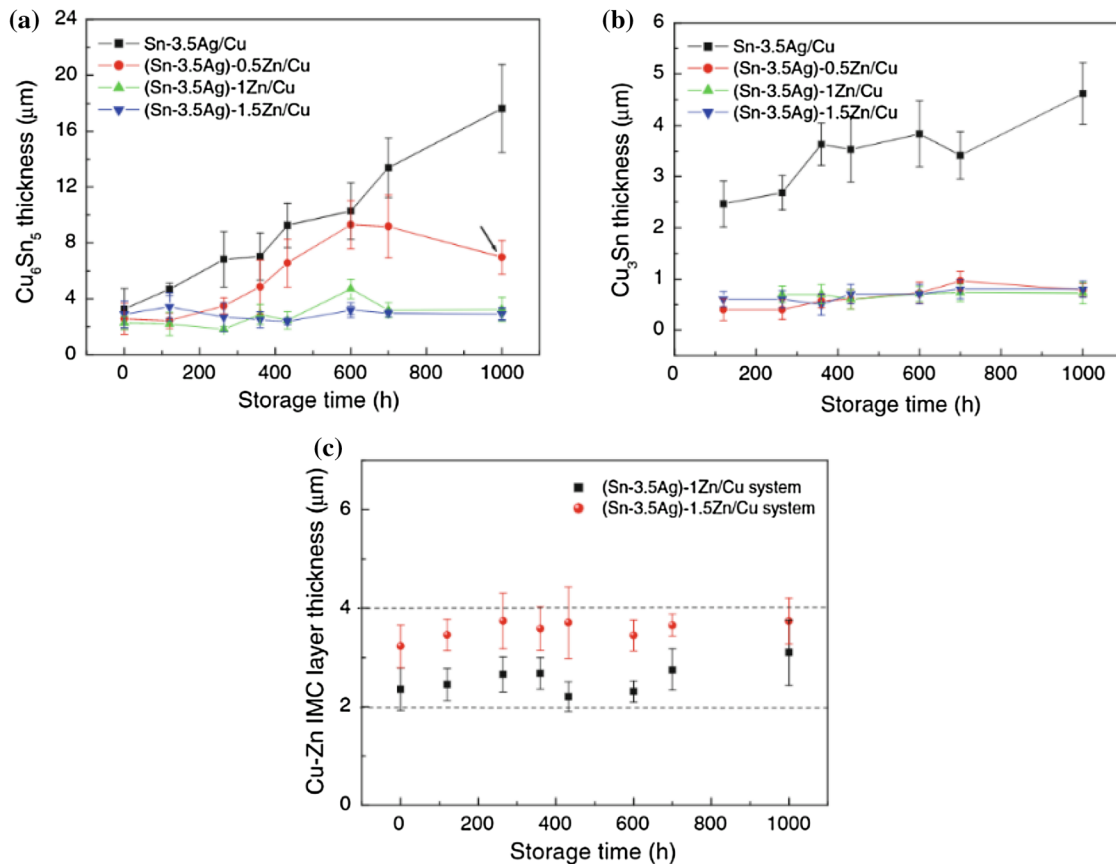


**Fig. 15** The thickness of IMC as a function of aging time: **a**  $\text{Cu}_6\text{Sn}_5/\text{Cu}$ , **b**  $\text{Cu}_3\text{Sn}/\text{Cu}$ , and **c**  $\text{Cu-Zn}/\text{Cu}$  interfaces. All the samples reflow at 260 °C for 60 s, and the storage temperature was 150 °C [61]

are many block compounds in the solder joints without aging treatment. After 150 h of aging treatment, IMC grow into irregular shapes in the matrix. After aging for 250 h, there is no obvious change in microstructure exclude some compounds precipitated in the solder joint. The results show that  $\text{Au}/\text{Sn-5Sb-1Cu-0.1Ni-0.1Ag}/(\text{Au})$  Ni solder joint is relatively stable, and the aging resistance is enhanced after all the matrix solders are consumed. As shown in Fig. 17, the IMC morphology of  $\text{Au}/\text{Sn-5Sb-1Cu-0.1Ni-0.1Ag}/(\text{Au})$  Ni solder joints changes with the increase of aging time. The morphology of IMC in the solder joint is layered structure without aging. Dele-Afolabi et al. [70] studied the effect of multi-walled carbon nanotubes (CNTs) on the Sn-5Sb/Cu solder joint. In the process of reflow soldering, a single  $\text{Cu}_6\text{Sn}_5$  IMC layer was formed in Sn-5Sb/Cu, Sn-5Sb-0.01CNT/Cu, Sn-5Sb-0.05CNT/Cu, and Sn-5Sb-0.1CNT/Cu solder joints. After isothermal aging treatment at 170 °C,  $\text{Cu}_6\text{Sn}_5$  and  $\text{Cu}_3\text{Sn}$  IMC layers are formed, of which Sn-5Sb-0.05CNT/Cu solder

joint had smallest IMC layer thickness and slowest growth rate, as shown in the Table 3. Since adding CNTs particles can handicap the diffusion of Sn atoms from the matrix, adding CNTs into the solder could effectively retard the evolution of IMC in the solder.

At 150 °C, the Sn-5Sb solders treated with electroless nickel immersion gold (ENIG), organic solderability preservatives (OSP), and immersion silver (ImAg) were subjected to heat treatment for 720 h, respectively [20]. The IMC structure of ordinary Sn-5Sb solder is similar to Sn-5Sb solder after OSP and ImAg surface treatment, and  $\text{Cu}_6\text{Sn}_5$  IMC and  $\text{Cu}_3\text{Sn}$  IMC are formed. However, as shown in Fig. 18,  $\text{Cu}_3\text{Sn}$  IMC is not formed in the IMC of Sn-5Sb solder after ENIG surface treatment. The growth kinetics of IMC can be expressed as Eq. (1):

$$Y = a_0 + At^n \quad (1)$$

In the formula,  $a_0$  is the thickness of IMC when  $t = 0$ ;  $Y$  is the thickness of IMC changing with time  $t$ ;



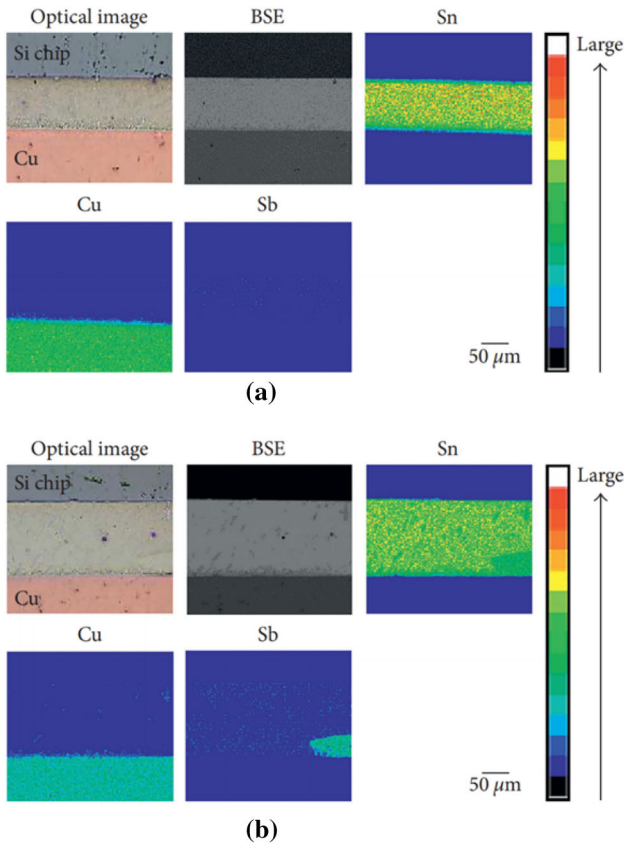
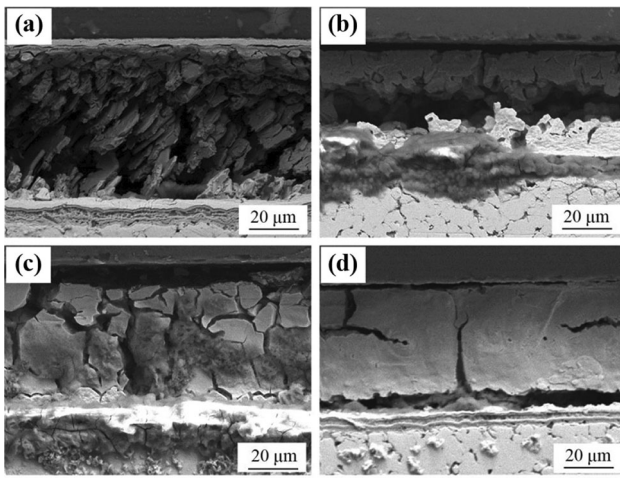


**Fig. 16** Optical image and back-scattered electron (BSE) images of cross section of **a**Sn-5Sb/Cu; **b** Sn-10Sb/Cu and EPMA mapping analysis [16]



Notes: (a) 0 h; (b) 150 h; (c) 250 h; (d) 350 h

**Fig. 17** IMC morphology of Au/Sn-5Sb-1Cu-0.1Ni-0.1Ag/(Au)Ni solder joint at 150 °C with deep etched [69]. **a** 0 h; **b** 150 h; **c** 250 h; **d** 350 h

$A$  is the growth constant; and  $n$  is the time index of IMC growth mechanism.  $n$  value depends on the way

of surface treatment. Therefore, the surface treatment will significantly affect the growth of IMC.

To summarize, it is found that the addition of appropriate amounts of alloying elements or nanoparticles to Sn-Ag and Sn-Sb solders can inhibit the growth of interfacial IMC. The addition of nanoparticles as high surface-active substances will concentrate at the grain boundaries, and the surface energy of the grain surface decreases, thus reducing the IMC growth rate.

## 4 Mechanical properties

Mechanical properties are one of the significant indexes to assess the performance of solder. Excellent mechanical properties can enhance the reliability of solder joints and prolong the service time [71], so it is very significant to research the mechanical properties of solder.

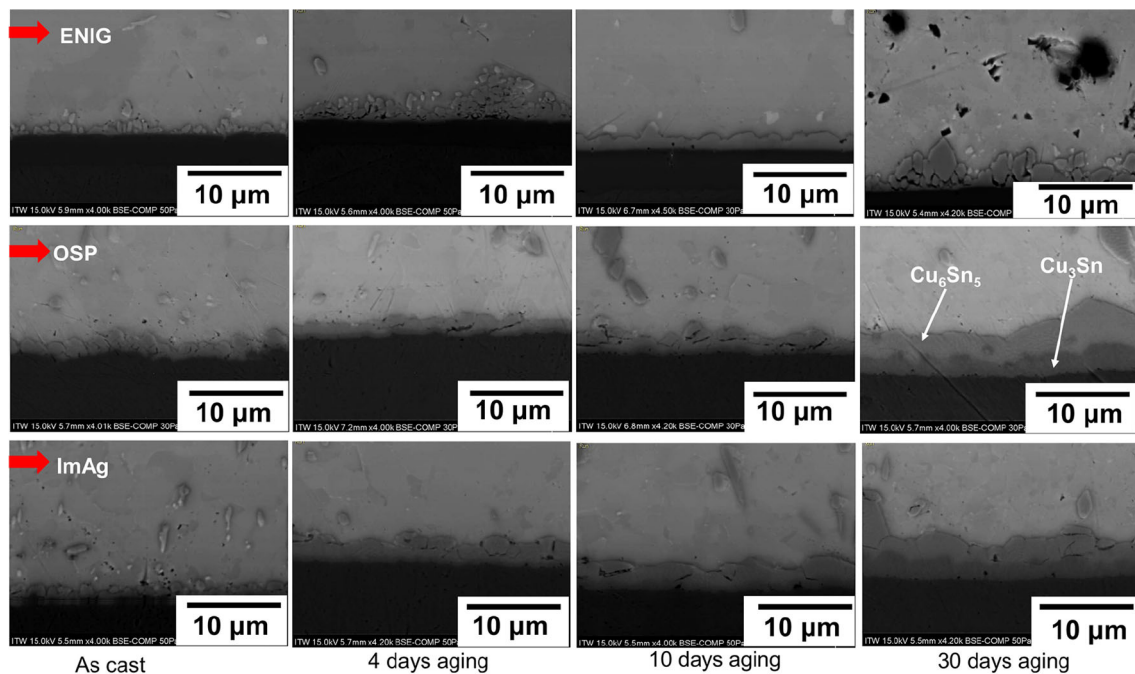
### 4.1 Sn-Ag

The Sn-3.5Ag solder has higher strength because of the high dislocation density during the cold-working. The yield strength (YS) of solder decreases significantly after annealing, which is mainly due to the growth of grain and the decrease of dislocation density of the solder after annealing [72]. On the basis of the fine grain strengthening theory, solder with small grain size has higher strength. Since the grain size of  $Ag_3Sn$  IMC is basically the same under all heat treatment conditions, the YS of Sn-3.5Ag is mainly determined by the grain size of Sn-rich phase. Chen et al. [73] observed that the shear strength of Sn-3.5Ag solder bump decreased by 5.3 wt.% after isothermal aging at 150 °C for 1500 h. When the temperature is 150 °C and the aging time is 720 h, the hardness of Sn-3.5Ag solder is reduced by 34%, mainly because the crystal grains of Sn-3.5Ag solder have undergone rapid growth and the process of particle coarsening [20].

The solder is finally applied to electronic devices, so it is significant to research the mechanical characteristics of solder joints. Rhee et al. [74] found that the peak shear stress and the flow stress of Sn-3.5Ag/Cu solder joint are proportional to temperature, and inversely proportional to the single shear stress. The shear band is mainly the deformation mechanism in microstructure of the solder at low temperature. The

**Table 3** Summary of average IMC thickness in all samples [70]

Aging time (h)	IMC thickness ( $\mu\text{m}$ )											
	Sn-5Sb			Sn-5Sb-0.01CNT			Sn-5Sb-0.05CNT			Sn-5Sb-0.1CNT		
	Total	$\text{Cu}_6\text{Sn}_5$	$\text{Cu}_3\text{Sn}$	Total	$\text{Cu}_6\text{Sn}_5$	$\text{Cu}_3\text{Sn}$	Total	$\text{Cu}_6\text{Sn}_5$	$\text{Cu}_3\text{Sn}$	Total	$\text{Cu}_6\text{Sn}_5$	$\text{Cu}_3\text{Sn}$
0	3.04	3.04	–	2.65	2.65	–	2.60	2.60	–	2.76	2.76	–
50	7.69	4.14	3.53	9.75	4.56	5.19	9.03	4.03	4.99	9.90	4.16	5.76
1000	11.67	5.72	5.95	9.75	4.56	5.19	9.03	4.03	4.99	9.90	4.16	5.76
1500	14.06	6.28	7.78	13.02	5.83	7.18	11.99	5.18	6.81	12.42	5.56	7.15

**Fig. 18** Microstructural evolution of IMC growth of Sn-5Sb solder on different finishes [20]

deformation is mainly grain boundary deformation in microstructure of the solder at high temperature of 125–150 °C. As shown in Fig. 19, high shear strain rate will cause concentrated deformation in the local area of the solder, and low shear strain rate will result in diffusion deformation in the local area of the solder.

Guo et al. [75] observed asymmetric growth of  $\text{Cu}_6\text{Sn}_5$  IMC in Cu/Sn-3.5Ag/Cu solder joints during reflowing for 40 min on a hot plate at 260 °C.  $\text{Cu}_6\text{Sn}_5$  IMC grew to 12.3  $\mu\text{m}$  at the cold end and 3.5  $\mu\text{m}$  at the hot end. The IMC occurred asymmetrical growth because of the temperature gradient in the solder joint when reflowing on the hot plate.  $\text{Ni}_3\text{Sn}_4$  IMC will be generated in the Cu/electroless Ni-P/Sn-

3.5Ag solder joints [47]. The growth of  $\text{Ni}_3\text{Sn}_4$  IMC and the expenditure of Cu will decrease the strength of Cu/electroless Ni-P/Sn-3.5Ag solder joints, causing brittle fracture at the  $\text{Ni}_3\text{Sn}_4$ /Sn-4.5Ag interface, as shown in Fig. 20. Therefore, many researchers will enhance the strength of solder joints by second strengthening method.

The creep property and thermal-mechanical fatigue resistance of Sn-4Ag-0.5Cu were better than Sn-3.5Ag solder because  $\text{Cu}_6\text{Sn}_5$  IMC could inhibit the grain boundary sliding under high-temperature creep and thermal mechanical fatigue cycle [59]. Keller et al. [76] carried out shear tests on Sn-3Ag-0.4Cu and Sn-3.7Ag-0.4Cu solders and found that Sn-3Ag-0.4Cu has higher strength because a large

**Fig. 19** Images of Sn-3.5Ag solder joint surfaces after shear tests for specimens deformed at the rate of simple shear strain of **a** 0.001 /s at 25 °C, **b** 0.1 /s at 25 °C, **c** 0.001 /s at 150 °C, and **d** 0.1 /s at 150 °C [74]

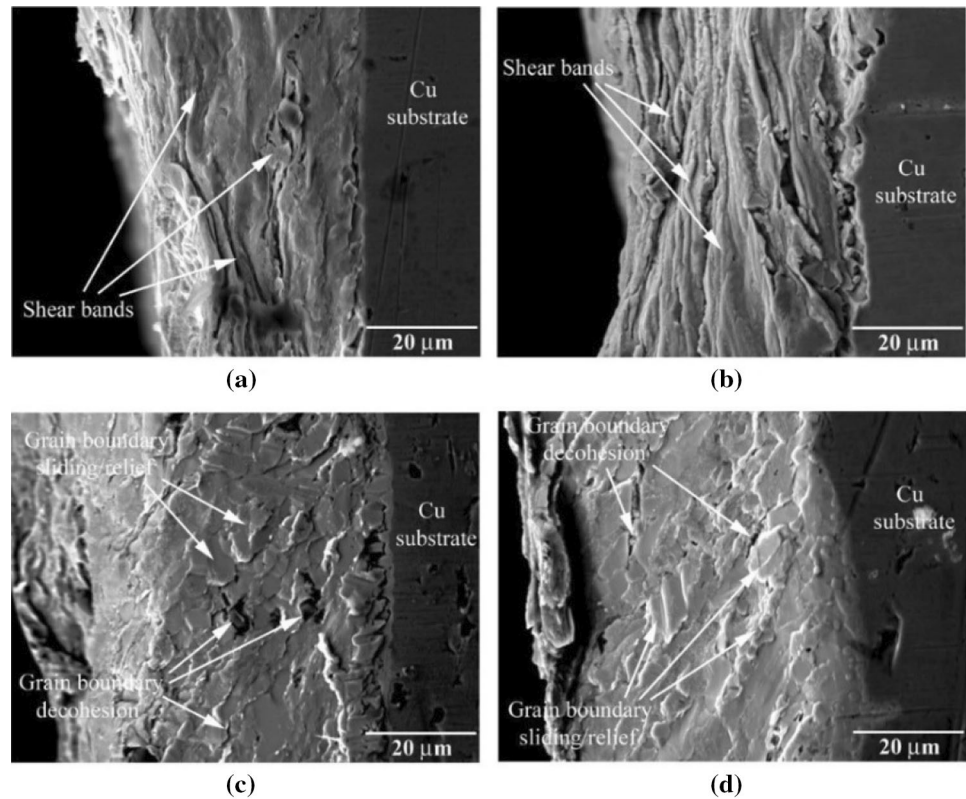
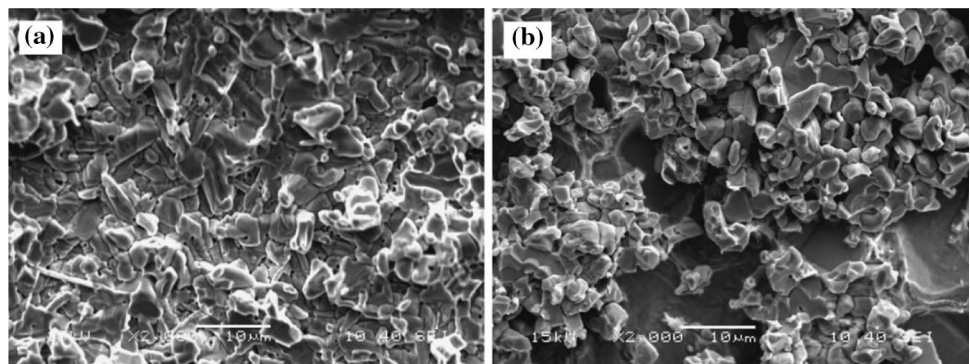


**Fig. 20** Fracture surfaces of the Cu/electroless Ni–P/Sn–3.5Ag solder joint aged at 180 °C for 400 h at the interface between **a**  $\text{Ni}_3\text{Sn}_4$  and **b** solder [47]



number of plate-like  $\text{Ag}_3\text{Sn}$  appeared in Sn-3.7Ag-0.4Cu, resulting in low strength of Sn-3.7Ag-0.4Cu solder. The tensile strength of Sn-3.5Ag, Sn-3.5Ag-0.75Cu, and Sn-3.5Ag-2Bi solders were studied by Shohji et al. [77]. The tensile strength of solder reduced with the decrease of strain rate and the increase of temperature. In the strain rate range of  $1.67 \times 10^{-4} \text{ s}^{-1}$  to  $1.67 \times 10^{-2} \text{ s}^{-1}$  and the temperature range of  $-40$  to  $120 \text{ °C}$ , the ductility of the solder is relatively stable. Witkin et al. [78] found that the addition of Bi greatly reduced the loss of strength of Sn–Ag–Cu or Sn–Ag solder during aging. The YS decreased by 50%, and the tensile strength of Sn-3Ag-

0.5Cu solder decreased by 37% after aging at  $150 \text{ °C}$  for 336 h. However, the microstructure of Sn-3.4Ag-4.8Bi solder has changed, but its YS and ultimate tensile strength (UTS) hardly changed, because the Bi element plays a role of solid solution strengthening and precipitation strengthening. Mahmudi et al. [23] found that adding 1.5 wt.% Sb element into Sn-3.5Ag solder can improve the strength and plasticity of solder. The reason for the improvement of the mechanical characteristics of the solder is that Sb has the effect of solid solution strengthening. The refinement of  $\text{Ag}_3\text{Sn}$  IMC in the solder plays the role of fine grain strengthening.



Besides trace elements, the addition of nanoparticles can enhance the reliability of solder joints. At different superimposed oscillation frequencies (0, 0.4, 0.9, and 1.3 Hz) and deformation temperatures (30, 50, 70, and 90 °C), the stress–strain curve of Sn-3.5Ag-ZnO solder is higher than Sn-3.5Ag solder, as shown in Fig. 21 [27], indicating that the addition of 0.3wt.% ZnO particles can significantly increase tensile strength of Sn-3.5Ag solder. Babaghorbani et al. [79] found that adding 0.7 vol% SnO<sub>2</sub> particles into Sn-3.5Ag solder can enhance the mechanical properties of the solder. Its YS increased by 18% and UTS increased by 31%. The addition of 0.05wt.% nano-Al<sub>2</sub>O<sub>3</sub> particles to Sn-3.6Ag solder could also enhance the shear strength and plasticity of the solder [63]. Adding an appropriate amount of ceramic particles in Sn-3.5Ag or Sn-3.5Ag-0.7Cu solder can enhance the

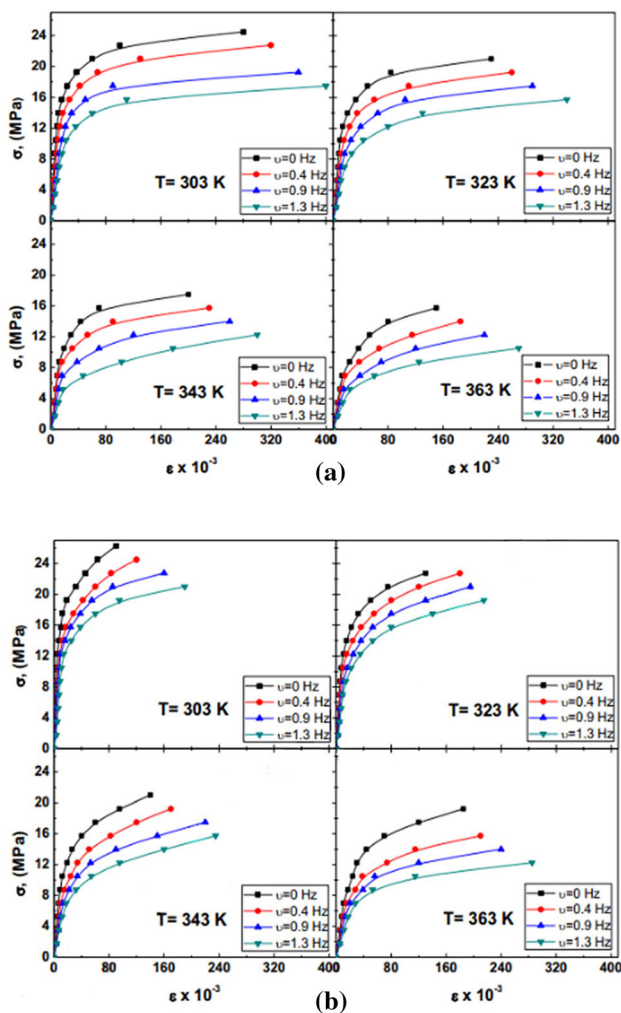


**Fig. 21** Stress–Strain curves for **a** Sn-3.5Ag **b** Sn-3.5Ag-0.3ZnO [27]

mechanical strength, but it will not affect the electrical resistivity [80].

## 4.2 Sn-Sb

In the case of a temperature of 150 °C and aging for up to 720 h, the hardness of the Sn-5Sb solder has almost no change [20]. At 150 °C, the Sn-5Sb solder was aged for 720 h, and the hardness of the solder was found to be almost unchanged. The main reason is that Sb has the effect of solid solution strengthening. Moreover, the Sn-Sb phase in Sn-5Sb solder is relatively stable at high temperature, which can hinder the dislocation movement of grains and maintain relatively stable mechanical properties [32]. Dias et al. [40] tested that the UTS, YS, and elongation ( $\delta$ ) of Sn-10Sb solder were 53 MPa, 44 MPa, and 16%, respectively. Compared with Sn-5Sb solder, Sn-10Sb solder has a better UTS and YS, but lower  $\delta$ . Lederer et al. [81] conducted mechanical bending fatigue tests on Cu-strip/Sn-Sb-Ag/DCB (commercial direct bonded copper) solder joints. Schematic of fatigue loading is shown in Fig. 22a. Figure 22b is the displacement diagram of sample. It was found that the crack growth rate was inversely proportional to the crack length in the fatigue test. Comparing Pb-Sn-Ag and Sn-Sb-Ag solders, it was found that the total mechanical strain of the two solders was similar. However, the Sn-Sb-Ag solder can resist higher stress because of the higher Young's modulus of Sn-Sb-Ag.

The UTS of Sn-5Sb, Sn-5Sb-0.7Ag, and Sn-5Sb-0.7Cu solders was 32.4, 34.3 and 40.0 MPa, respectively, at 90 °C and  $1.2 \times 10^{-2} \text{ s}^{-1}$  strain rate. The elongations were 60%, 62.5%, and 69.0%, respectively. New Cu<sub>6</sub>Sn<sub>5</sub> IMC and Ag<sub>3</sub>Sn IMC were formed in  $\beta$ -Sn matrix of Sn-5Sb-0.7Cu solder and Sn-5Sb-0.7Ag solder, respectively. The elastic modulus of Cu<sub>6</sub>Sn<sub>5</sub> IMC is higher than that of Ag<sub>3</sub>Sn, so the deformation resistance and elongation of Sn-5Sb-

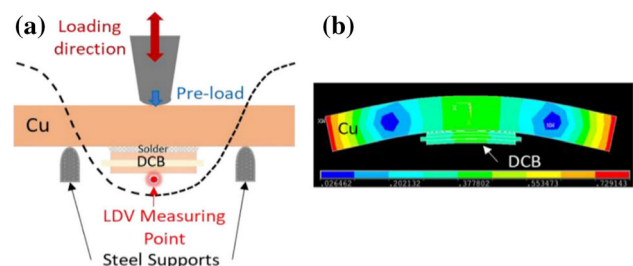


**Fig. 22** **a** Schematic of fatigue loading, **b** Displacement plot of a sample subjected to bending fatigue [81]

0.7Cu solder are better than Sn-5Sb and Sn-5Sb-0.7Ag solder [32]. The microhardness of Sn-10Sb solder is 203.49 MPa, and the microhardness increases to 313.72 MPa after adding 2 wt.% In element which is mainly because of the influence of fine grain strengthening. The Young's modulus of Sn-10Sb solder increased from 52.25 GPa to 65.22 GPa by adding 2 wt.% In, mainly due to the presence of hard IMC. The tensile fracture strength increased from 10.21 GPa to 11.42 GPa, and the yield strain increased from  $1.29 \times 10^{-3}$  to  $1.60 \times 10^{-3}$ , because of the reaction of the second phase strengthening [35]. Adding 1.5 wt.% Bi and 1.5 wt.% Cu into Sn-5Sb solder can enhance the strength and plasticity of solder [82]. The elongations of Sn-5Sb-1.5Bi, Sn-5Sb-1.5Cu, and Sn-5Sb solders are 153%, 138%, and 113% at the strain rate of  $5 \times 10^{-4} \text{ s}^{-1}$ , respectively. Sn-5Sb-1.5Bi solder has better mechanical properties. The improvement of strength is due to the solid solution strengthening influence of Bi element and the evolution of  $\text{Cu}_6\text{Sn}_5$  IMC. The plasticity is improved because the addition of alloying elements can refine grains. Therefore, adding trace elements can enhance the mechanical characteristics of the Sn-Sb solders.

Besides trace elements, nanoparticles can also be added. Dele-Afolabi et al. [83] found that the shear strength of Sn-5Sb-0.01CNT solder is 29% higher than Sn-5Sb solder. Because of the excellent mechanical properties of carbon nanotubes and the uniform distribution of carbon nanotubes in the matrix, it can inhibit the growth of IMC. The morphology of Sn-CNT in the Sn-5Sb-0.01CNT and the Sn-5Sb-0.05CNT solder joint is shown in Fig. 23. It will cause the agglomeration of carbon nanotubes when the CNTs content is high (0.05–0.1 wt.%), thus causing the weak bonding between solder and CNTs particles.

Adding 0.2 wt.% graphene oxide nanosheets (GONSs) into Sn-5Sb-1.0Ag (SSA510) solder can improve the UTS, deformation resistance, and plasticity of the solder, mainly because a small amount of GONSs particles could hinder the growth of  $\beta$ -Sn, Sn-Sb, and  $\text{Ag}_3\text{Sn}$ , thus improving the mechanical properties of the solder [38]. Adding 5 vol.% of  $0.3 \mu\text{m}$   $\text{Al}_2\text{O}_3$  nanoparticles could enhance the mechanical characteristics of the Sn-1.7Sb-1.5Ag solder [84]. Geranmayeh et al. tested the mechanical characteristics of the solder by shear impact test (STP). Compared with Sn-1.7Sb-1.5Ag solder, the YS and UST of the composite solder increased by 4.8 MPa and 6.2 MPa at room temperature,

respectively. The improvement of mechanical characteristics is mainly due to the mismatch between matrix and thermal expansion coefficient (CTE), and partly because of the Orowan strengthening mechanism of  $\text{Al}_2\text{O}_3$  particles, as shown in the formula (2):

$$\sigma = \frac{2Gb}{\lambda} \quad (2)$$

where  $G$  is the shear modulus,  $b$  is the vector dislocation,  $\lambda$  is the average distance of grain dispersion, and  $\sigma$  is the yield stress. As shown in the Fig. 24 [37], the addition of 0.3 wt.% ZnO nanoparticles can increase the UTS and YS of Sn-5Sb-1.5Ag solder. In addition, the UTS and YS of the solder increase with the increase of strain rate and the decrease of temperature. This behavior is attributed to the effect of particle size refinement, the effect of thermal expansion mismatch, Orowan strengthening, and adsorption of the nanoparticles ZnO.

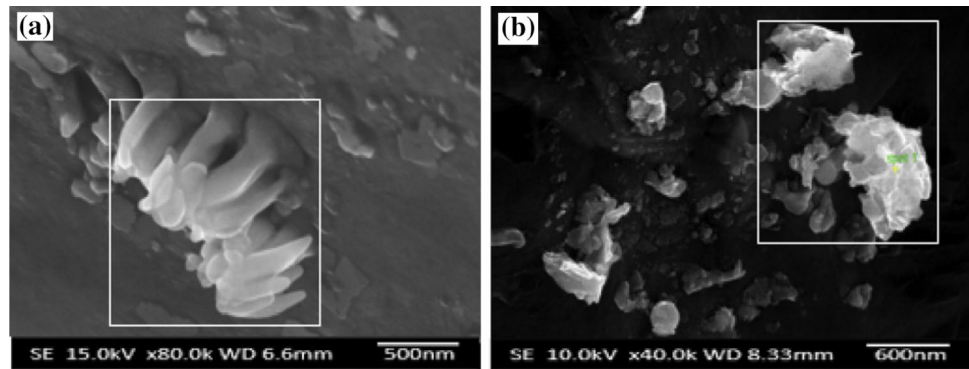
Rocha et al. [85] carried out a horizontal directional solidification experiment on a single-phase Sn-2Sb solder. It was found that the Vickers-hardness (HV) changes with the change of grain size, the effect of cellular crystal, and dendrite on the microhardness can be seen, as shown in Fig. 25. In the cellular region, the microhardness remains unchanged, and in the dendrite region, the microhardness decreases with the increase of dendrite spacing, which can be expressed by the Hall–Petch formula (3):

$$H = 65 + 52.9\lambda_1^{-0.5} \quad (3)$$

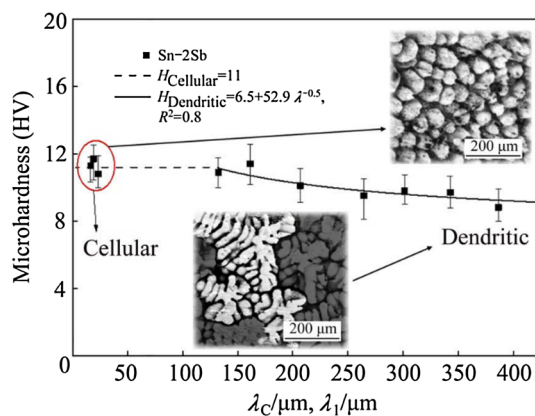
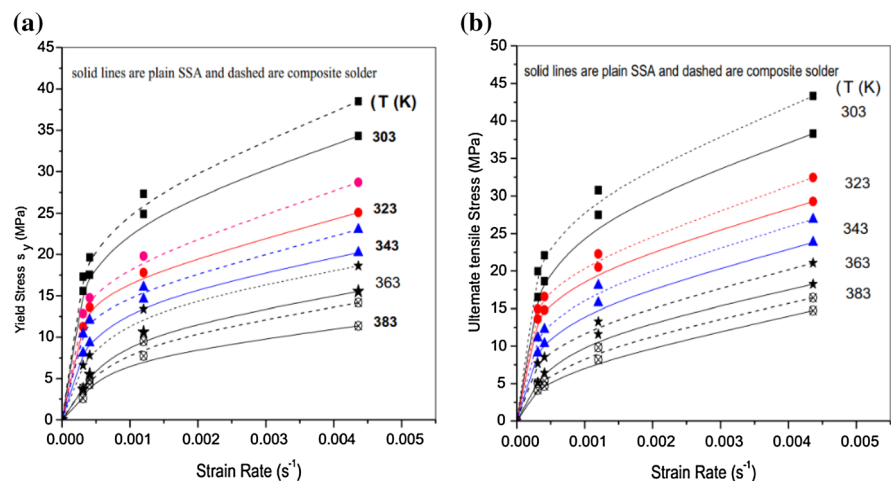
where  $\lambda_1$  is primary dendritic arm, and  $H$  is microhardness. Gouda et al. [86] researched the influence of annealing temperature on the mechanical characteristics of Sn-5Sb solder. The HV of Sn-5Sb solder was  $12.9 \text{ N/mm}^2$  and YS was 43 MPa before annealing. After annealing at  $120 \text{ }^\circ\text{C}$  for 60 min, HV and YS increased to  $14.7 \text{ N/mm}^2$  and 49 MPa, respectively. After annealing at  $200 \text{ }^\circ\text{C}$  for 60 min, HV and YS increased to  $19.1 \text{ N/mm}^2$  and 63.7 MPa, respectively. The improvement of mechanical properties is that Sn-5Sb solder has more the Sn-Sb IMC, higher lattice parameters, larger grain size, and the lower lattice strain.

Table 4 recaps the influence of trace elements and nanoparticles on the mechanical properties of Sn-Ag/Sn-Sb solder. Table 4 reveals that adding trace elements or nanoparticles can improve UTS, YS, and plasticity. It is found that adding trace elements or

**Fig. 23** FE-SEM images of the fracture morphology of Sn-CNT of **a** Sn-5Sb-0.01CNT and **b** Sn-5Sb-0.05CNT in the solder matrix [83]



**Fig. 24** Strain rate dependence of **a** YS, **b** UTS for the samples [37]



**Fig. 25** The evolution of microhardness with cell/primary dendrite arm spacing [85]

nanoparticles into the solder can improve the mechanical characteristics of Sn-Ag/Sn-Sb solder. According to the theory of fine grain strengthening, the finer the grain, the more grain boundaries are contained per unit volume, and the greater the resistance to dislocation movement, thus improving the strength of the brazing material. According to

dispersion strengthening, the addition of dispersive particles will impede the dislocation movement, so as to achieve the effect of strengthening. This is the reason why the addition of alloying elements or nanoparticles can improve the mechanical properties of Sn-Ag and Sn-Sb solders.

## 5 Wettability

Wettability of solder is the wetting and spreading ability of molten solder on substrate, which is determined by surface energy and interface energy of solid/liquid interface [2]. Many researchers began to research how to enhance the wettability of solder.

### 5.1 Sn-Ag

The wettability between molten solder and substrate is defined by the wetting angle  $\theta$ , as shown in Fig. 26. The Young equation is as follows [87],



**Table 4** Effect of trace element or nanoparticles addition on the mechanical properties of Sn-Ag/Sn-Sb solder

Solder	Element	Wt.%	UTS	YS	Shear strength	plasticity	References
Sn-Ag	Cu	0.75	↑				[77]
	Bi	2.0	↑↑				[77]
	Sb	1.5	↑(4%)	↑		↑↑(84%)	[23]
	Cu, Bi	0.5, 3.3	↑↑	↑↑			[78]
	Bi	4.8	↑	↑			[78]
	ZnO nanoparticles	0.3	↑	↑↑(30%)			[27]
	SnO <sub>2</sub> nanoparticles	0.7vol%	↑(18%)	↑↑(31%)			[78]
Sn-Sb	Cu	0.7	↑↑(23%)			↑(15%)	[32]
	Ag	0.7	↑(6%)			↑(4%)	[32]
	In	2.0		↑↑(24%)			[35]
	Bi	1.5	↑↑			↑↑(35%)	[82]
	Cu	1.5	↑			↑↑(22%)	[82]
	CNTs	0.01				↑↑(29%)	[83]
	GONSs	0.2	↑			↑	[38]
	Al <sub>2</sub> O <sub>3</sub> nanoparticles	5vol%				↑(16%)	[84]
	ZnO nanoparticles	0.3	↑	↑			[37]

$$\cos \theta = \frac{(\gamma_{SF} - \gamma_{SL})}{\gamma_{LF}} \tag{4}$$

where  $\gamma_{SF}$ ,  $\gamma_{SL}$  and  $\gamma_{LF}$  are solid–gas, liquid–solid, and gas–liquid surface tension, respectively, and  $\theta$  is the wetting angle.

Xu et al. [88] researched the effect of temperature on the wettability of Sn-3.5Ag and pure Sn solder on Cu substrate. The surface tension of Sn-3.5 Ag solder is inversely proportional to temperature. The surface tension of Sn-3.5Ag solder is higher than pure Sn in the range of 250–300 °C. Therefore, the weldability of Sn-3.5Ag solder on Cu substrate is higher than pure Sn. Sn-Ag solder has different wettability on different substrates. Liu et al. [89] studied the wettability of Sn-3.5Ag on Cu and Cu substrates plated with Au, Pd, and Au/Pd. It was found that the wetting angles of the solder were 17° and 15° on the Au/Cu and Au/Pd/Cu-plated substrates, respectively. Therefore, plating a layer of Au on the Cu substrate can enhance the wettability. However, the wetting angle is 35° on

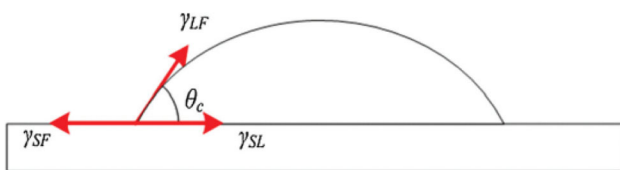


**Fig. 26** The surface tension diagram under equilibrium [87]

the Pd/Cu substrate, which is close to the wetting angle on the Cu substrate. Therefore, plating a layer of Pd on the Cu substrate cannot enhance the wettability of the solder. The wetting characteristics of Sn-3.5Ag solder on Ag/Ni and Ni-plated 304 stainless steel (304SS) substrates were explored by Nayak et al. [90]. It was found that the wetting angle of the solder was 18.73° on the Ag/Ni-plated 304SS substrate, and the wetting angle was 24.5° on the Ni-plated 304SS substrate. The presence of many Fe–Cr–Sn IMC will inhibit the further wetting of the solder at the interface of the Sn-3.6Ag/Ni/304SS solder joint, leading to a larger contact angle.

Different forming processes will also change the wettability of solder. Liu et al.[29] found that the wettability of Sn-3.5Ag prepared by RSP is better compared with CRP. The spreading area of Sn-3.5Ag solder prepared by RSP is 31.8 mm<sup>2</sup>, 31% larger than CRP, as shown in Fig. 27. The reason is as follows: firstly, the later melting phase inhibits the flow of the earlier melting phase in casting–rolling solder. Secondly, the low liquidus temperature of solder prepared by RSP increases the superheat and fluidity. Thirdly, the melt of solder is more uniform in the rapidly solidified solder, which is accessible to bond with the atoms on the matrix, reducing the surface energy and wetting angle. These factors improve the wettability of solder prepared by RSP.

Tikale et al. [63] added 0.01–0.5 wt.%  $\text{Al}_2\text{O}_3$  nanoparticles to Sn-3.6Ag solder to improve the wettability of the solder. By adding 0.5 wt.%  $\text{Al}_2\text{O}_3$  particles into Sn-3.6Ag solder, the spreading area of solder increased from 28 to 36  $\text{mm}^2$ . The main reason is that the grain boundary/interfacial energy was changed by the presence of surface-active nanoparticles, thereby reducing the surface tension of the molten solder and the interfacial tension between the solder and substrate. This leads to an increase in the diffusion capacity of the molten solder, thereby improving the wettability of the solder. Hsiao et al. [91] prepared Sn-3.5Ag-0.2Cu, Sn-3.5Ag-0.5Cu, and Sn-3.5Ag-1.0Cu solders by chemical reduction method. It was found that the wetting angles of the three solders (Sn-3.5Ag-0.2Cu, Sn-3.5Ag-0.5Cu, and Sn-3.5Ag-1.0Cu) on Cu substrate were 28°, 24°, and 22°, respectively. Adding 1 wt.% Ni in Sn-3.5Ag solder can effectively enhance the wettability of solder, and the spreading area increased by 15% [92]. But the wettability begins to decrease when the content of Ni exceeds 1 wt.%, because Ni and its surrounding IMC increase the viscosity of molten solder and reduce the fluidity of solder.

## 5.2 Sn-Sb

In Sn-Sb solders, Sb element is the surface aggregation element in Sn-Sb solder. The surface tension of solder decreases with the increase of Sb content in Sn-Sb solder [93]. The wetting angles of Sn-5.5Sb solder on copper, nickel, and stainless steel substrates were 15°, 27°, and 21°, respectively [16]. Therefore, Sn-5.5Sb solder has the best wettability on Cu substrate. The wetting angles of Sn-5.5Sb and Sn-10Sb solders on a carbon steel substrate were 45.1° and 43.7°, respectively, as shown in Fig. 28 [40].

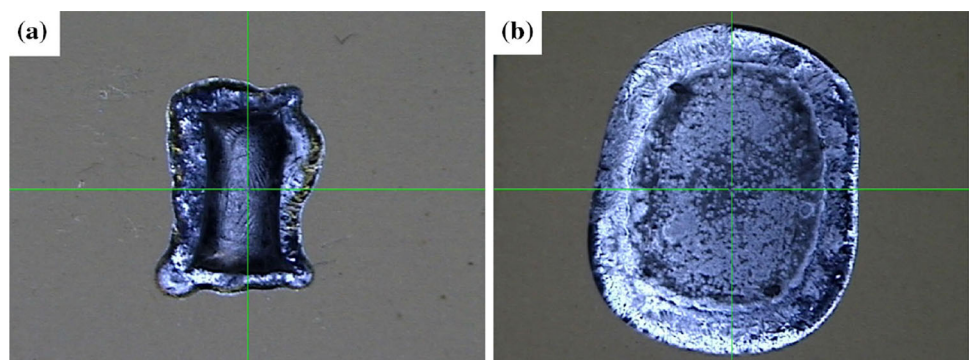
EL-Bahay et al. [94] found that the wetting angles of Sn-5Sb solder on  $\text{CuZn}_{30}$  and Cu substrates were 41° and 40° at 300 °C, but the wetting angles on Al and glass substrates were 115° and 118°, respectively. This means solder melts are more suitable for copper or brass-coated substrates. The wetting angle of solder with the addition of Bi element decreases gradually. Adding 1, 2, and 3 wt.% Bi into Sn-10Sb decreased the wetting angles of solder from 35° to 33°, 29°, and 18°, respectively [33]. The wetting angle was 32.8° between Sn-5Sb solder and Cu substrate. Adding 0.01 wt.% CNTs particles in the solder can reduce the wetting angle by 2.1°. Adding 0.05 wt.% CNTs can reduce the wetting angle by 4.5°. Adding 0.1 wt.% CNTs can decrease the wetting angle by 3.6°. It was observed that the wettability of Sn-5Sb-0.05CNT solder is relatively good [83]. The formation of IMC is the key to control the wettability of the interface, and adding CNTs particles can hinder the diffusion of Sn atoms, thereby inhibiting the evolution of IMC. Therefore, CNTs particles can reduce the wetting angle of solder.

Table 5 outlines the influence of trace element and nanoparticles on the wettability of Sn-Ag/Sn-Sb solder and the different wettability of Sn-Ag/Sn-Sb solder on different substrates. Table 5 shows that adding trace elements or nanoparticles can enhance the wettability of solder. One of the conditions to ensure the reliability of solder joints is good wettability between solder and substrate, so it is significant to research how to enhance the wettability of solder.

## 6 Melting behavior

Melting property is one of the important properties of solder. The melting temperature of solder determines the peak temperature of solder reflow soldering. The

**Fig. 27** Typical images of two Sn-3.5Ag solders after spreading experiment: **a** CRP; **b** RSP [29]



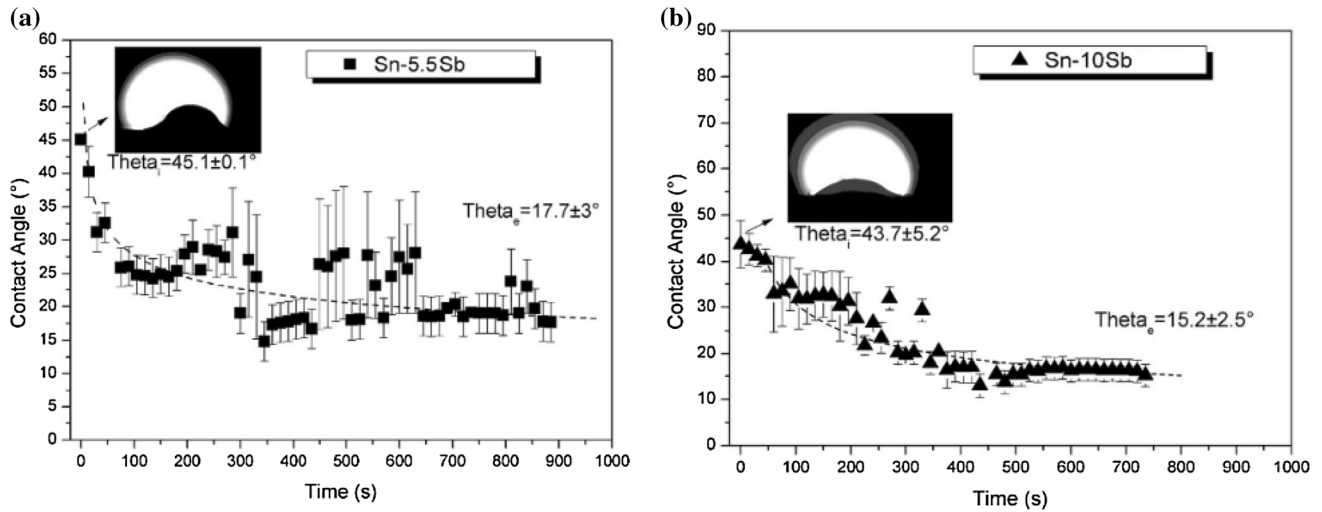


**Fig. 28** The evolution of contact angle during the wetting tests of Sn-5.5Sb and Sn-10Sb solders on a carbon steel substrate [40]

**Table 5** Effect of trace elements or nanoparticles addition on the mechanical properties of Sn-Ag/Sn-Sb solder

Solder	Substrate	Element	Wt. %	Forming process	Spreading area(mm <sup>2</sup> )	Contact angle	References
Sn-Ag	Au/Cu					17°	[89]
	Au/Pd/Cu					15°	[89]
	Pd/Cu					35°	[88]
	Ag/Ni					18.73°	[90]
	Ni-plated 304SS					24.5°	[90]
	Au-plated			RSP	31.8		[29]
	Au-plated			CRP	24.8		[29]
	Cu	Al <sub>2</sub> O <sub>3</sub> nanoparticles	0.5			36	[63]
Sn-Sb	Cu	Cu	0.2,0.5,1.2			28°, 24°, 22°	[91]
	Cu	Ni	1		121		[92]
	Cu					15°	[16]
	Ni					27°	[16]
	Stainless steel					21°	[16]
	Cu	Bi	1,2,3			33°,29°,18°	[33]
	Cu	CNTs	0.01,0.05,0.1			30.7°,28.3°,29.2°	[83]

melting behaviors of solder are similar to Sn–Pb solder, which is useful to the continuation of the actual welding measure and equipment [2]. What’s more, it can diminish the harm of circuit board components generated by the heat output during brazing.

### 6.1 Sn-Ag

Melting property is one of the important properties of solder. The melting point of solder determines the peak temperature of solder reflow soldering. The eutectic point of Sn-Ag is obtained at the 3.5 wt. % silver concentration and the melting point of Sn-

3.5Ag solder is 221 °C [18]. Kotadia et al. [61] found that adding 1.5 wt.% Zn into Sn-3.5Ag solder can reduce the melting point from 219.15 °C to 216.3 °C, and the addition of 2 wt.% Al increases the melting point of the solder by 6.81 °C. However, adding Zn and Al element decreased the undercooling of the solder by 13.5 °C and 8.88 °C, respectively, as shown in the Fig. 29. The melting points of Sn-3.5Ag-0.2Cu, Sn-3.5Ag-0.5Cu, and Sn-3.5Ag-1.0Cu solders prepared by the chemical reduction were 215.45 °C, 214.97 °C, and 214.76 °C, respectively [91]. The melting point of Sn-Ag-Cu solder is effectively decreased below 215 °C by the chemical reduction.



Song et al. [95] found that adding 3 wt.% In element can significantly reduce the undercooling and the melting point of Sn-3.5Ag and increase the solid–liquid phase line range from 10.2 °C to 14.2 °C. The reason is that In element is incorporated into Sn dendrite, eutectic Sn, and Ag<sub>3</sub>Sn phase, which helps to reduce the formation temperature of these phases. Tikale et al. [63] found that adding 0.01–0.1 wt.% nano-Al<sub>2</sub>O<sub>3</sub> particles to Sn-3.6Ag solder can decrease the melting temperature and pasty range of the solder. As shown in Table 6, the melting characteristics of the solder have been significantly improved by adding 0.05 wt.% Al<sub>2</sub>O<sub>3</sub> nanoparticles, but when the content of Al<sub>2</sub>O<sub>3</sub> nanoparticles is increased to 0.1 wt.%, the Al<sub>2</sub>O<sub>3</sub> nanoparticles increase the agglomeration of the nanoparticles and reduce the amount of active material dispersed, so that the addition of the beneficial effects of nanoparticles are reduced.

The forming process of solders has influence on the melting point. Liu et al. [29] found that contrasted with the CRP, the Sn-3.5Ag solder prepared by the RSP has a lower melting point, the solid phase temperature is reduced by 1.37 °C, and the liquid phase temperature is reduced by 1.44 °C. The main reason is that the grain size of the brazing filler metal prepared by the RSP is smaller, which adds the surface energy and lowers the melting temperature. In

addition, the lattice constant and atomic spacing of Sn-based solid solution were increased because of Ag in Sn matrix, thereby reducing the interatomic force and lowering the melting temperature.

## 6.2 Sn-Sb

The liquid temperature of Sn-5Sb is about 240 °C and that of Sn-10Sb solder is 250 °C [16]. The melting temperature of Sn-5Sb and Sn-10Sb meets the requirement of high-temperature solder for the melting point, so Sn-5Sb and Sn-10Sb are potential replacements for high-temperature lead solder. Many researchers further enhance the melting characteristics of lead-free solders by alloying.

A small amount of Ag and Cu can reduce the melting temperature of the solder. The melting points of Sn-5Sb and Sn-5Sb-0.7Cu are 239.2 °C and 233.8 °C, respectively. There are two endothermic peaks in Sn-5Sb-0.7Ag solder. As shown in Fig. 30, the first endothermic peak is 228.7 °C and the second endothermic peak is 236.9 °C. The addition of 0.7Cu and 0.7Ag increased the width of the liquid–solid two-phase region from 3.9 °C to 6.9 °C and 14.2 °C, respectively [32].

Adding Ag and Au reduced the melting points of Sn-5Sb from 240 °C to 216 °C and 203.5 °C,

**Fig. 29** DSC thermal profile of solder during heating and cooling cycles: **a** and **b** with the addition of Zn to Sn-3.5Ag solder; **c** and **d** with the addition of Al to Sn-3.5Ag solder, during heating and cooling at 10 °C min<sup>-1</sup> [61]

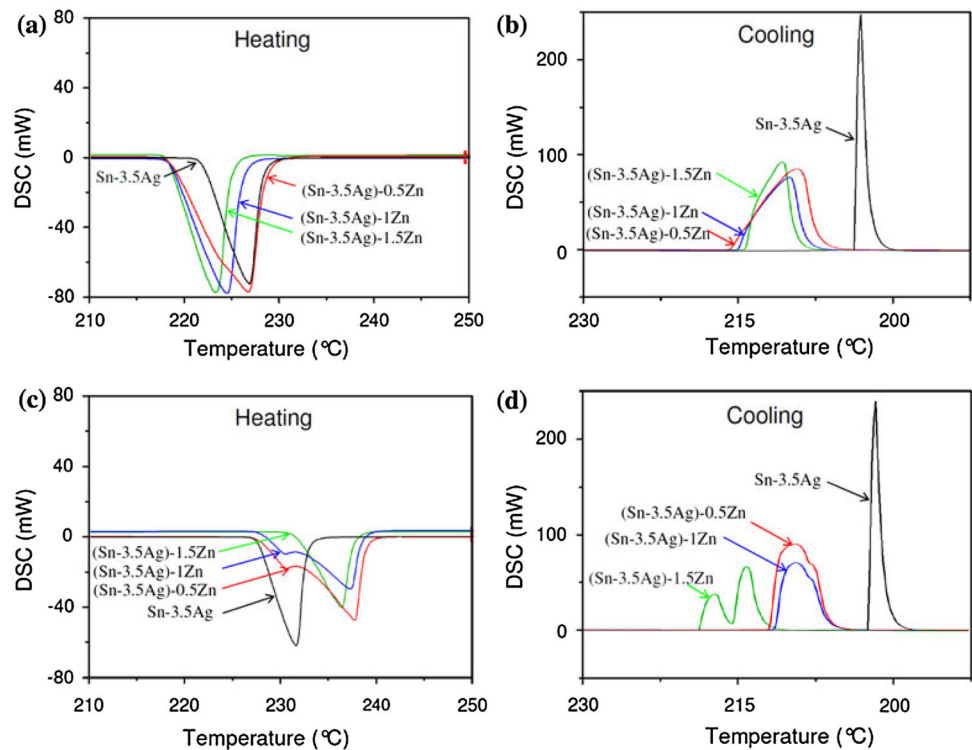


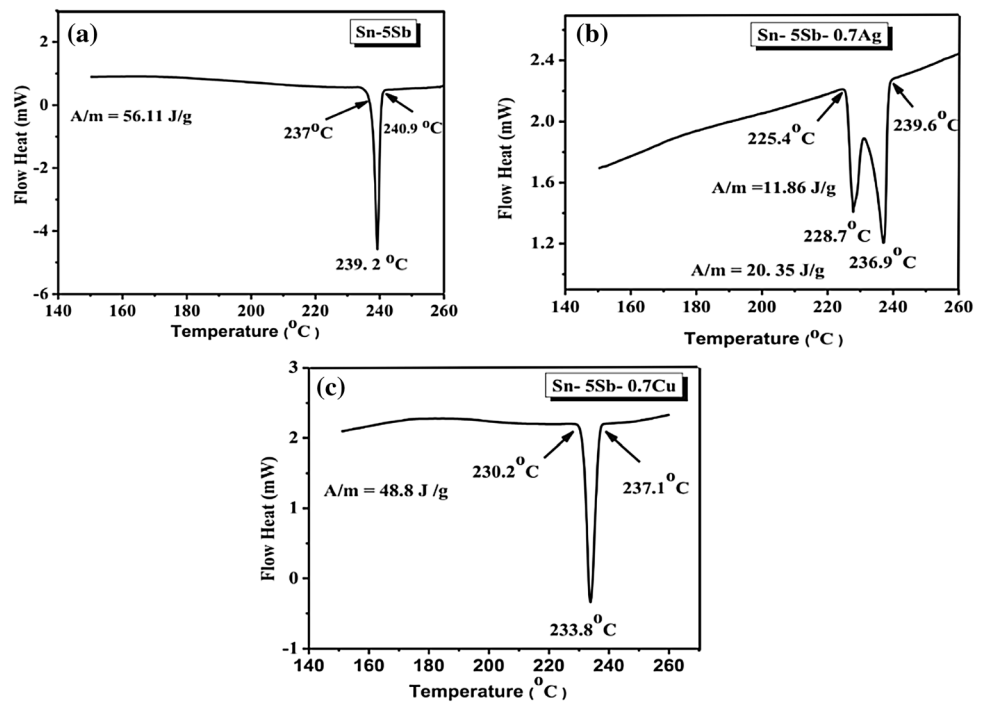
**Table 6** Peak melting temperature, pasty range, and melting temperature range of Sn-3.6Ag solder with different content of nano-Al<sub>2</sub>O<sub>3</sub> particles [63]

Solder composition	T <sub>Onset</sub> heating(°C)	T <sub>Pesk</sub> heating(°C)	T <sub>Endset</sub> heating(°C)	Pasty range (°C)	Melting temperature range(°C)
Sn-3.6Ag	221.84	225.77	228.17	6.33	3.93
Sn-3.6Ag-0.01Al <sub>2</sub> O <sub>3</sub>	221.44	224.99	226.98	5.54	3.55
Sn-3.6Ag-0.05Al <sub>2</sub> O <sub>3</sub>	220.58	224.05	226.01	5.43	3.47
Sn-3.6Ag-0.1Al <sub>2</sub> O <sub>3</sub>	220.6	224.21	226.52	5.92	3.61
Sn-3.6Ag-0.5Al <sub>2</sub> O <sub>3</sub>	220.71	224.66	227.19	6.48	3.95

respectively [31]. Adding Ag will make the melting heat of the solder from 140.5 to 191.4 J/g, but the addition of Au will reduce the alloy to 87.1 J/g. Therefore, Sn-5Sb-1.5Au solder is a relatively energy-saving solder. Chen et al. [96] found that adding Ag element into Sn-5Sb solder could significantly reduce the melting temperature of solder. Compared with Sn-5Sb solder, the melting point of Sn-5Sn-5Ag solder decreased by 10.5 °C. Based on this result, under the melting point of Sn-5Sb solder, the long contact time of Sn-5Sb/Ag is easier to reduce the melting point of solder. Therefore, the long welding time of Sn-5Sb/Ag should be avoided. The melting point of Sn-5Sb is 244.4 °C, and the melting points of Sn-5Sb solders decreased to 233.7 °C, 231 °C, and 231.9 °C by adding 1, 3, and 5 wt.% Ag, respectively, as shown in Fig. 31 [97]. The main reason is the increase of the Ag<sub>3</sub>Sn IMC. The melting temperature of Sn-10Sb solder was

decreased from 240 °C to 233 °C by adding 2 wt.% In due to the refinement of crystal size. For eutectic alloy, the pasty range (the solidus–liquidus distance) is zero, and Sn-5Sb-2In solder pasty range is 22.22 °C, relatively narrow [35]. This behavior leads to the solder left-off during solidification. Sobhy et al. [38] found that adding 0.5 wt.% GONSs to Sn-5Sb-1Ag could increase the melting point of solder from 222 °C to 223.4 °C. The reason is that GONSs particles can be used as delay sites in the solidification process of solder. Mansour et al. [37] found that the addition of 0.3 wt.% ZnO nanoparticles in Sn-5Sb-1.5Ag (SSA) solder reduced the melting temperature of the solder by 0.08 °C. The pasty range is explained as the difference between the solidus and liquidus temperatures. The paste range of SSA solder and SSA composite solder is within 6.55 °C, which is smaller than Sn-5Sb (10 °C) and Sn–Pb (11.5 °C). The melting

**Fig. 30** DSC heating curves for a Sn–5Sb, b Sn–5Sb–0.7Ag, and c Sn–5Sb–0.7Cu solder [32]



temperature of Sn-7.5Sb solder solidified at 15.7 m/s cooling rate was 245 °C, while the melting temperature of Sn-7.5Sb solder solidified at 30.7 m/s cooling rate was 243.5 °C. A higher cooling rate can refine the grain, thereby reducing the melting point [98].

## 7 Creep behavior

Creep refers to the slow and permanent deformation of solder under stress. Lead-free solder is more prone to creep deformation during service compared with Sn–Pb solder. Creep is one of the critical reasons for solder joint failure in electronic components [2], so it is necessary to study how to reform the creep characteristics of lead-free solders.

### 7.1 Sn-Ag

According to the creep fatigue test, it was found that the creep fatigue process of Sn-4Ag/Cu solder joints included strain hardening stage, steady deformation stage, and accelerated fracture stage [99]. With the increasing number of cycles, the strain concentration appeared at the interface of Cu<sub>6</sub>Sn<sub>5</sub> IMC and began to produce microcrack. The strain on the solder joint is caused by plastic deformation. The creep mechanism of solder is mainly dislocation climbing. Dutta et al.

[100] investigated the creep behavior of Sn-3.5Ag solder with rapid cooling microstructure by indentation creep test. β-Sn matrix and Ag<sub>3</sub>Sn IMC existed in Sn-3.5Ag solder in the reflow process. Under low stress, the solder slip deformation occurs, and the slip velocity is controlled by the diffusion of Ag element. Under high stress, the creep of solder is controlled by dislocation and Ag<sub>3</sub>Sn IMC. The creep deformation of Sn-3.5Ag solder under low stress was mainly caused by slip and climb mechanisms. The interface reaction of liquid Sn-2Ag/Ni solder joints at 230–250 °C was investigated by Taneja et al. [101]. It was found that the solder joint formed Ni<sub>3</sub>Sn<sub>4</sub> IMC with a smooth surface and a scallop shape in the short isothermal aging time (1–4 min). After 4 min of reaction, the average thickness was about 1–1.5 μm. When the reaction time is longer (> 1 h), the scallop-shaped Ni<sub>3</sub>Sn<sub>4</sub> IMC gradually transforms into an irregular growth form. After 4 h of reaction, the thickness of Ni<sub>3</sub>Sn<sub>4</sub> IMC is about 4–7 μm. When the stress index of Ni<sub>3</sub>Sn<sub>4</sub> IMC is between 0.35 and 0.40, the activation energy is 21.07 ± 2.28 kJ/mol, indicating that the evolution of Ni<sub>3</sub>Sn<sub>4</sub> IMC is dominated by grain boundary diffusion.

Adding trace elements can enhance the creep resistance of solder. The creep mechanisms of Sn-3.0Ag-0.5Cu and Sn-3.4Ag-1.0Cu-3.3Bi and Sn-3.4Ag-4.8Bi solders are all dislocation climbing [102]. The creep resistance of Sn-3.0Ag-0.5Cu solder is higher than the other two solders containing Bi element, but after aging treatment, the creep resistance of Sn-3.0Ag-0.5Cu solder is the worst. It shows that Sn-3.4Ag-1.0Cu-3.3Bi and Sn-3.4Ag-4.8Bi solders are less affected by aging. The activation energies of Sn-3.5Ag, Sn-3.5Ag-0.75Cu, and Sn-3.5Ag-2Bi solders are 46.6, 47.3 and 61.6 kJ/mol, respectively. These values indicate that the creep mechanism of these solders is dislocation slip [77]. The creep resistance of Sn-4Ag/Cu, Sn-4Ag-0.5Cu/Cu, and Sn-4Ag-1.0Cu/Cu are higher than Sn-37Pb/Cu, mainly because fine Ag<sub>3</sub>Sn IMC has the effect of dispersion strengthening in lead-free solder joints [103]. The creep performance of Sn-Ag-Cu is better than Sn-Ag at low temperatures. The main reason is that the addition of Cu element precipitates tiny η-Cu<sub>6</sub>Sn<sub>5</sub> IMC in the Sn matrix. Huang et al. [104] established a new creep constitutive model of Sn-3Ag-0.5Cu solder as shown in the formula (5)–(7):

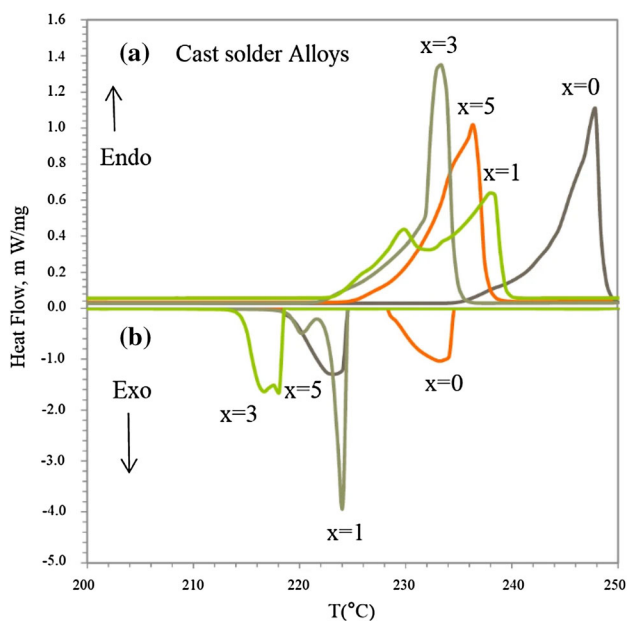


**Fig. 31** DSC curves of Sn-5Sb-1Ag, Sn-5Sb-3Ag and Sn-5Sb-5Ag with temperature under **a** heating and **b** cooling processes [97]



$$\dot{\epsilon} = \left[ A_0 + B_0 \exp\left(-\frac{C_0}{T}\right) \right] \sigma \text{ where } \sigma < \sigma_V \tag{5}$$

$$\dot{\epsilon} = A_1 (\sinh B_1 \sigma)^n \exp\left(\frac{-Q}{RT}\right) \text{ when } \sigma \geq \sigma_V \tag{6}$$

$$\sigma_V = b_0 + b_1 \exp(b_2 T) \tag{7}$$

where  $\sigma$  is the equivalent stress,  $Q$  is the activation energy,  $R$  is the universal gas constant,  $T$  is the absolute temperature value, and  $T_R$  is 0 °C; it was found that this model could improve the existing constitutive model of Sn-Ag-Cu solder and is more suitable prediction of thermal fatigue life of MPM (microelectronic power module). The room-temperature creep curves of lead-free solder under three different loads (0.098, 0.245, and 0.490 N) are shown in the Fig. 32. It can be observed that the indentation strain is proportional to the loading time. The curve shows two areas from the creep indentation point of view. The creep rate is variable at the end of the first stage. The second stage is named the steady-state stage, and the creep rate is comparatively stable. Due to the low load and loading time, the third stage did not occur[21]. Guo et al. [105] added 15 vol% Ag and 20 vol% Cu<sub>6</sub>Sn<sub>5</sub> particles into Sn-3.5Ag, and found that the solder containing Cu<sub>6</sub>Sn<sub>5</sub> particles had relatively good creep properties, but adding Ag element could not improve the creep resistance of Sn-3.5Ag solder. The main reason is that Cu<sub>6</sub>Sn<sub>5</sub> particles can promote the homogenization deformation of solder joints and reduce the strong deformation of solder joints in a single part, so that the solder joints begin to the tertiary creep at a low strain level. Although Ag particles can also make the solder joint deform uniformly, the creep performance of the composite solder containing Ag has not been improved because of the strong bonding ability between Ag and solder.

### 7.2 Sn-Sb

Zhang et al. [106] analyzed the reliability of Sn-3.5Ag and Sn-5Sb solders in chip scale package (CSP) with finite element analysis and the Garofalo–Arrhenius creep model. It was found that the fatigue life of Sn-Sb was longer than Sn-Ag solder. Mathew et al. [107] researched the creep behaviors of Sn, Sn-3.5Ag, and Sn-5Sb solders within the temperature range of room temperature to 200 °C. The stress indexes of Sn, Sn-3.5Ag, and Sn-5Sb solders were 7.6, 5.0, and 5.0, respectively, and the creep activation energies were

60.3, 60.7, and 44.7 kJ/mol, respectively. On the basis of the stress index and activation energy, the creep deformation mechanism in Sn and Sn-3.5Ag solders is dislocation climbing controlled by lattice diffusion, and viscous glide in Sn-5Sb. The main reason for the good creep resistance of Sn-5Sb solder is the existence of Sn-Sb IMC [108]. Mahmudi et al. [109] researched the effect of homogenization on creep properties of Sn-5Sb by Vickers indentation test. The solder was homogenized for 24 h in the temperature range of 48 °C-132 °C. The creep mechanism of Sn-5Sb solder under uniform condition was dislocation creep. Under non-uniform conditions, the creep mechanisms under low stress state and high stress state are dislocation slip and dislocation creep, respectively. Geranmayeh et al. [110] carried out a long-time Vickers indentation test at room temperature to explore the creep performance of Sn-5Sb. To study the influence of homogenization on the creep characteristic of materials, some samples were homogenized at 505 °C for 24 h. Based on the steady-state power law model, the stress indexes of the solder under the conditions of homogenized wrought (HW), unhomogenized wrought (UW), homogenized cast (HC), and unhomogenized cast (UC) were tested. It was found that the main creep mechanism under HW condition was dislocation creep, while the main creep mechanism was dislocation creep under other conditions. The values of  $n$  and  $Q$ , as is known to all, are generally used to decide deformation mechanisms [37]. Mahmudi et al. [111] found that under the low stress of cast conditions, the creep activation energy

**Table 7** The activation energy ( $Q$ ) and stress exponent ( $n$ ) of Sn-5Sb, Sn-5Sb-0.7Ag, and Sn-5Sb-0.7Cu solders at low and high stresses [32]

Solder	Temperature (°C)	$n$ values		$Q$ (kJ/mol)
		$\sigma_{Low}$	$\sigma_{High}$	
Sn-5Sb	25	7.5	7.5	89.0
	90	7.2	7.2	
	120	6.8	6.8	
Sn-5Sb-0.7Ag	25	9.5	5.1	63.3
	90	7.7	4.5	
	120	7.2	3.8	
Sn-5Sb-0.7Cu	25	8.0	4.2	104.0
	90	6.2	4.2	
	120	4.1	3.5	

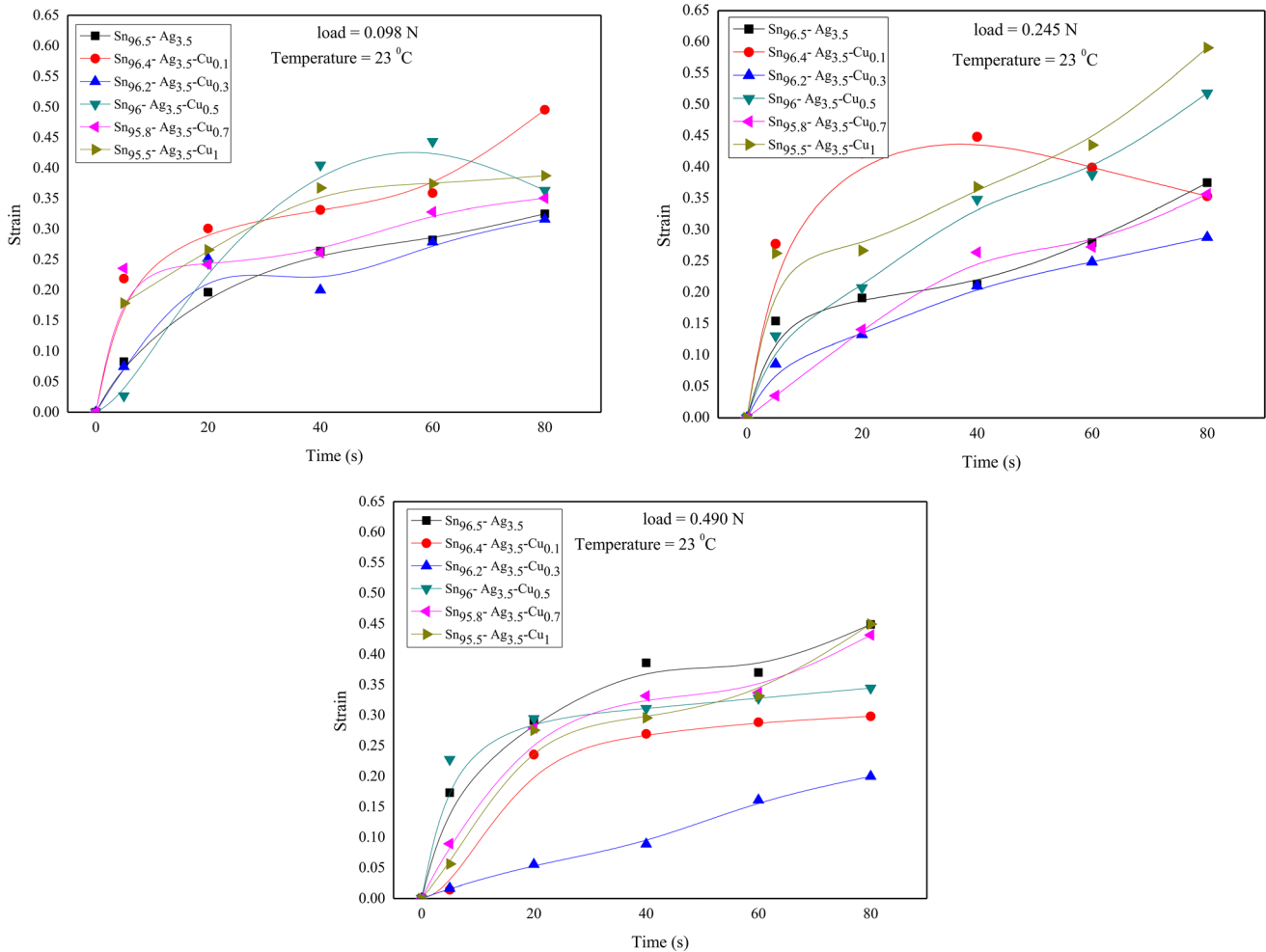


**Fig. 32** Strain variation versus loading time of the samples [21]

was 53.8 kJ/mol, and the stress index of Sn-5Sb solder was 5.4, indicating that the effective creep mechanism was dislocation climbing. Under the high stress of cast conditions, the creep activation energy is 75.8 kJ/mol, and the stress index is 11.4. The creep mechanism is mainly the dislocation creep mechanism. Under wrought conditions, the creep activation energy of Sn-5Sb is 41.3 kJ/mol, and the stress index is 2.8, indicating that the main creep mechanism of solder under wrought conditions is grain boundary sliding.

At 25 °C, the creep characteristic of the three solders (Sn-5Sb, Sn-5Sb-3.5Ag, and Sn-5Sb-1.5Au) was tested under a load of 41.5 MPa. Sn-5Sb-1.5Au solder had higher creep resistance and fracture life compared with Sn-5Sb and Sn-5Sb-3.5Ag, mainly because hard AuSn<sub>4</sub> IMC hindered the dislocation movement to a large extent [31]. Park et al. [112] researched the creep properties of Sn-8.0Sb-3.0Ag by the creep

experiment which was carried out at 175 °C under the load of 2.45 MPa on Sn-8.0Sb-3.0Ag solder. It was found that the Sn-8.0Sb-3.0Ag solder will form a slender Ag<sub>3</sub>Sn structure, and Ag<sub>3</sub>Sn can inhibit the dislocation movement, thereby improving the creep resistance of the solder. Shalaby [33] found that adding Ag and Bi element reduced the creep rate of Sn-5Sb solder and improved the creep properties of solder. The reason is that adding Bi can enhance the effect of solid solution strengthening, and adding Ag element, which plays a role in particle strengthening, forms a new Ag<sub>3</sub>Sn. The excellent creep behavior of Sn-5Sb-1.5Bi solder is better compared with Sn-5Sb-1.5Ag and Sn-5Sb-1Ag-1Bi, which indicates that Bi element is more effective in improving the creep resistance of the solder. As the temperature increases from 25 °C to 127 °C, the stress exponents of Sn-5Sb, Sn-5Sn-1.5Bi, and Sn-5Sb-1.5Cu solders are from 7.1 to 4.4, 7.8 to 3.7, and 6.2 to 3.4, respectively [82].

During high-temperature deformation, the stress index decreases with the increase of temperature, which is relevant to the instability of microstructure. According to the activation energy and stress index of each solder, dislocation climbing is the main deformation mechanism of Sn-5Sb solder. However, for Sn-5Sn-1.5Bi and Sn-5Sb-1.5Cu solders, dislocation climbing is the main deformation mechanism at low temperature, and grain boundary diffusion is the main deformation mechanism at high temperature, respectively. The tensile creep behavior of Sn-5Sb, Sn-5Sb-0.7Ag, and Sn-5Sb-0.7Cu solders was characterized by  $n$  values [32]. Under high stress levels and low temperature range (25–70 °C),  $n$  value was in the range of 5.1–10.7, when under low stress level and high temperature (120 °C),  $n$  value was roughly 5–5.7. The data of stress index and activation energy indicate that dislocation climbing dominated by lattice diffusion is the creep mechanism of solder, as shown in Table 7.

## 8 Conclusions

In this review, it is noted that introducing trace elements or nanoparticles into solders is beneficial to improve the properties of Sn-Ag and Sn-Sb solder. Additionally, changing the cooling conditions of the solder can also improve its performance. The addition of trace elements or nanoparticles in appropriate amounts can refine the microstructure of solders and inhibit the growth of interfacial IMC, thus strengthening the mechanical properties of solders and the reliability of the solder joint. The addition of some particles can reduce the surface tension of solders and thus improve the wettability. Nevertheless, the research on these two solders is still on the experimental stage and cannot be fully applied in the electronic industry. The evolutions of IMC have significant influences on the mechanical properties and creep resistance of solders, but the studies on the interfacial reaction and IMC evolution of Sn-Sb solders are not enough. Therefore, the interfacial IMC of Sn-Sb solder joints can be studied more in future. Although Sn-Ag and Sn-Sb solders have good mechanical properties, the melting point of the two solders is lower compared with other high-temperature solders such as Au-Sn, Au-Ge, Zn-Al, and so on. Low melting point is not conducive to the secondary reflow soldering and will be limited in high-

temperature applications. If Sn-Ag and Sn-Sb are used as high-temperature solders, the melting behaviors of solders at high temperature can be further improved.

## Acknowledgements

The present work was under support of Natural Science Foundation of Jiangsu Province (BK20211351), the Key project of State Key Laboratory of Advanced Welding and Joining (AWJ-19Z04).

## Author contribution

Xi Wang involved in data curation and writing—original draft preparation. Liang Zhang and Mu-lan Li participated in writing—reviewing and editing.

## Data availability

The datasets supporting the conclusions of this article are included within the article.

## Declarations

**Conflict of interest** The authors declare that they have no known competing financial interests or personal relationships that could have appeared to influence the work reported in this paper.

## References

1. H.R. Kotadia, P.D. Howes, H.M. Mannan et al., A review: On the development of low melting temperature Pb-free solders[J]. *Microelectron. Reliab.* **54**(6–7), 1253–1273 (2014)
2. M. Zhao, L. Zhang, Z.Q. Liu et al., Structure and properties of Sn-Cu lead-free solders in electronics packaging[J]. *Sci. Technol. Adv. Mater.* **20**(1), 421–444 (2019)
3. Z. Liang, K.N. Tu, Structure and properties of lead-free solders bearing micro and nano particles[J]. *Mater. Sci. Eng. R. Rep.* **82**, 1–32 (2014)
4. S. Cheng, C.M. Huang, M. Pecht, A review of lead-free solders for electronics applications [J]. *Microelectron. Reliab.* **75**, 77–95 (2017)
5. M.L. Li, L. Zhang, N. Jiang et al., Materials modification of the lead-free solders incorporated with micro/nano-sized particles: A review [J]. *Mater. Design* **197**, 109224 (2021)



6. Y.B. Park, G.T. Park, B.R. Lee et al., Solder volume effect on electromigration failure mechanism of Cu/Ni/Sn-Ag Microbump [J]. *IEEE Trans. Compon. Packaging Manuf. Technol.* **99**, 1–1 (2020)
7. Y. Wang, Y. Wang, L. Ma et al., Effect of Sn grain c-axis on Cu atomic motion in Cu reinforced composite solder joints under electromigration [J]. *J. Electron. Mater.* **49**(3), 2159–2163 (2020)
8. Z. Yao, S. Jiang, L. Yin et al., Effects of joint height on the interfacial microstructure and mechanical properties of Cu-Cored SAC305 solder joints[J]. *J. Electron. Mater.* **49**(9), 5391–5398 (2020)
9. L. Zhang, W.M. Long, F.J. Wang, Microstructures, interface reaction, and properties of Sn–Ag–Cu and Sn–Ag–Cu–0.5CuZnAl solders on Fe substrate[J]. *J. Mater. Sci. Mater. Electron.* **31**(9), 6645–6653 (2020)
10. A.K. Gain, L. Zhang, Nanoindentation creep, elastic properties, and shear strength correlated with the structure of Sn-9Zn-0.5nano-Ag alloy for advanced green electronics[J]. *Metals* **10**(9), 1137 (2020)
11. Q. Zhang, F. Hu, Z. Song, Transient soldering reaction mechanisms of SnCu solder on CuNi nano conducting layer and fracture behavior of the joint interfaces[J]. *J. Electron. Mater.* **49**(5), 3383–3390 (2020)
12. N. Jiang, L. Zhang, W.M. Long et al., Influence of doping Ti particles on intermetallic compounds growth at Sn58Bi/Cu interface during solid–liquid diffusion[J]. *J. Mater. Sci.: Mater. Electron.* **32**(1), 3341–3351 (2021)
13. Y. Wei, Y. Liu, L. Zhang et al., Effects of endogenous Al and Zn phases on mechanical properties of Sn58Bi eutectic alloy[J]. *Mater. Charact.* **175**(5), 111089 (2021)
14. V. Chidambaram, J. Hattel, J. Hald, High-temperature lead-free solder alternatives[J]. *Microelectron. Eng.* **88**(6), 981–989 (2010)
15. G. Zeng, S. McDonald, K. Nogita, Development of high-temperature solders: Review[J]. *Microelectron. Reliab.* **52**(7), 1306–1322 (2012)
16. K. Tatsuya, S. Ikuo, N. Yusuke, Effect of power cycling and heat aging on reliability and IMC growth of Sn-5Sb and Sn-10Sb solder joints[J]. *Adv. Mater. Sci. Eng.* **2018**, 1–6 (2018)
17. S.W. Chen, C.H. Wang, S.K. Lin et al., Phase diagrams of Pb-free solders and their related materials systems[J]. *J. Mater. Sci.: Mater. Electron.* **18**(1/3), 19–37 (2007)
18. Z. Liang, C.W. He, Y.H. Guo et al., Development of SnAg-based lead free solders in electronics packaging—ScienceDirect[J]. *Microelectron. Reliab.* **52**(3), 559–578 (2012)
19. K. Kobayashi, I. Shohji, H. Hokazono, Tensile and fatigue properties of miniature size specimens of Sn-5Sb lead-free solder[J]. *Mater. Sci. Forum* **879**, 2377–2382 (2017)
20. M. Hasnine, B. Tolla, N. Vahora, Microstructural evolution and mechanical behavior of high-temperature solders: Effects of high-temperature aging[J]. *J. Electron. Mater.* **6**, 1–11 (2017)
21. R.M. Shalaby, M. Kamal, E.A.M. Ali et al., Microstructural and mechanical characterization of melt spun process Sn-3.5Ag and Sn-35.Ag-xCu lead-free solders for low cost electronic assembly[J]. *Mater. Sci. Eng. A Struct. Mater.* **690**, 446–452 (2017)
22. F. Guo, S. Choi, J.P. Lucas et al., Microstructural characterisation of reflowed and isothermally-aged Cu and Ag particulate reinforced Sn-3.5Ag composite solders[J]. *Solder. Surf. Mount Technol.* **13**(1), 7–18 (2001)
23. R. Mahmudi, S. Mahin-Shirazi, Effect of Sb addition on the tensile deformation behavior of lead-free Sn–3.5Ag solder alloy[J]. *Mater. Design* **32**(10), 5027–5032 (2011)
24. J. Wan, Y. Liu, W. Chen et al., Effect of the addition of In on the microstructural formation of Sn–Ag–Zn lead-free solder[J]. *J. Alloy. Compd.* **463**(1–2), 230–237 (2008)
25. J. Peng, Y. Liu, W. Chen et al., Effect of high-temperature annealing on the microstructural formation of Sn–3.7Ag–0.9Zn–x Al lead-free solder[J]. *J. Mater. Sci. Mater. Electron.* **20**(2), 139–143 (2009)
26. J. Shen, Y.C. Liu, Y.J. Han et al., Strengthening effects of ZrO<sub>2</sub> nanoparticles on the microstructure and microhardness of Sn-3.5Ag lead-free solder[J]. *J Electro Mater* **35**(8), 1672–1679 (2006)
27. M. Sobhy, Effects of torsional oscillation on tensile behavior of Sn–3.5wt% Ag alloy with and without adding ZnO nanoparticles[J]. *Mater. Sci. Eng. A* **610**, 237–242 (2014)
28. S. Wiese, K.J. Wolter, Microstructure and creep behaviour of eutectic SnAg and SnAgCu solders[J]. *Microelectron. Reliab.* **44**(12), 1923–1931 (2004)
29. S. Liu, Z. Hu, J. Xiong et al., Effects of forming processes on the microstructure and solderability of Sn-3.5Ag eutectic solder ribbons as well as the mechanical properties of solder joints[J]. *J. Electron. Mater.* **46**(11), 6737 (2017)
30. A.A. El-Daly, A.Z. Mohamad, A. Fawzy et al., Creep behavior of near-peritectic Sn-5Sb solders containing small amount of Ag and Cu[J]. *Mater. Sci. Eng. A* **528**(3), 1055–1062 (2011)
31. A.A. El-Daly, Y. Swilem, A.E. Hammad, Creep properties of Sn-Sb based lead-free solder alloys[J]. *J. Alloy. Compd.* **471**(1–2), 98–104 (2009)
32. A.A. El-Daly, A. Fawzy, A.Z. Mohamad et al., Microstructural evolution and tensile properties of Sn-5Sb solder alloy containing small amount of Ag and Cu[J]. *J. Alloy. Compd.* **509**(13), 4574–4582 (2011)

33. M. Kamal, E.S. Gouda, Decomposition behavior and properties for tin-antimony alloy with bismuth content[J]. *Radiat. Eff. Defects Solids* **161**(7), 427–431 (2006)
34. A.R. Geranmayeh, G. Nayyeri, R. Mahmudi, Microstructure and impression creep behavior of lead-free Sn–5Sb solder alloy containing Bi and Ag[J]. *Mater. Sci. Eng. A* **547**, 110–119 (2012)
35. R.M. Shalaby, Influence of indium addition on structure, mechanical, thermal and electrical properties of tin–antimony based metallic alloys quenched from melt[J]. *J. Alloy. Compd.* **480**(2), 334–339 (2009)
36. M.M. Mansour, G. Saad, L.A. Wahab et al., Indentation creep behavior of thermally aged Sn-5wt%Sb-1.5wt%Ag solder integrated with ZnO nanoparticles[J]. *J. Mater. Sci. Mater. Electron.* **30**, 8348–8357 (2019)
37. M.M. Mansour, A. Fawzy, L.A. Wahab et al., Tensile characteristics of Sn–5wt%Sb–1.5wt%Ag reinforced by nano-sized ZnO particles[J]. *J. Mater. Sci. Mater. Electron.* **30**, 4831–4841 (2019)
38. M. Sobhy, A.M. El-Refai, A. Fawzy, Effect of graphene oxide nano-sheets (GONSs) on thermal, microstructure and stress–strain characteristics of Sn-5wt% Sb-1wt% Ag solder alloy[J]. *J. Mater. Sci. Mater. Electron.* **27**(3), 2349–2359 (2016)
39. E.A. Eid, A.M. Deghady, A.N. Fouda, Enhanced microstructural, thermal and tensile characteristics of heat treated Sn-50Sb-03Cu (SSC-503) Pb-free solder alloy under high pressure[J]. *Mater. Sci. Eng.* **743**, 726–732 (2019)
40. M. Dias, T.A. Costa, B.L. Silva et al., A comparative analysis of microstructural features, tensile properties and wettability of hypoperitectic and peritectic Sn-Sb solder alloys[J]. *Microelectronics Reliability* **81**, 150–158 (2018)
41. L. Zhang, Z.Q. Liu, Inhibition of intermetallic compounds growth at Sn–58Bi/Cu interface bearing CuZnAl memory particles (2–6  $\mu\text{m}$ ) [J]. *J. Mater. Sci. Mater. Electron.* **31**(1), 2466–2480 (2020)
42. J.J. Yu, C.A. Yang, Y.F. Lin et al., Optimal Ag addition for the elimination of voids in Ni/SnAg/Ni micro joints for 3D IC applications[J]. *J. Alloy. Compd.* **629**, 16–21 (2015)
43. B. Guo, A. Kunwar, C. Jiang et al., Synchrotron radiation imaging study on the rapid IMC growth of Sn–xAg solders with Cu and Ni substrates during the heat preservation stage[J]. *J. Mater. Sci. Mater. Electron.* **29**(1), 589–601 (2018)
44. H. Ma, A. Kunwar, B. Guo et al., Effect of cooling condition and Ag on the growth of intermetallic compounds in Sn-based solder joints[J]. *Appl. Phys.* **A122**(12), 1052.1–1052.10 (2016)
45. C. Yu, J.S. Chen, K.Y. Wang et al., Suppression effect of Cu and Ag on Cu<sub>3</sub>Sn layer in solder joints[J]. *J. Mater. Sci. Mater. Electron.* **24**(11), 4630–4635 (2013)
46. M.O. Alam, Y.C. Chan, Solid-state growth kinetics of Ni<sub>3</sub>Sn<sub>4</sub> at the Sn–3.5Ag solder/Ni interface[J]. *J. Appl. Phys.* **98**(12), 14–485 (2005)
47. A. Kumar, C. Zhong, Influence of solid-state interfacial reactions on the tensile strength of Cu/electroless Ni–P/Sn–3.5Ag solder joint[J]. *Mater. Sci. Eng. A* **423**(1–2), 175–179 (2006)
48. J.W. Yoon, J.H. Bang, C.W. Lee et al., Interfacial reaction and intermetallic compound formation of Sn–1Ag/ENIG and Sn–1Ag/ENEPIG solder joints[J]. *J. Alloy. Compd.* **627**, 276–280 (2015)
49. S. Tian, Y. Liu, Q. Ma et al., Intermetallics-induced directional growth of Sn whiskers in Sn-3.5Ag coating on Al substrate[J]. *Appl. Surf. Sci.* **539**, 148135 (2021)
50. Y. Yao, J. Zhou, F. Xue et al., Interfacial structure and growth kinetics of intermetallic compounds between Sn-3.5Ag solder and Al substrate during solder process[J]. *J. Alloy. Compd.* **682**, 627–633 (2016)
51. M.Y. Xiong, L. Zhang, Interface reaction and intermetallic compound growth behavior of Sn-Ag-Cu lead-free solder joints on different substrates in electronic packaging[J]. *J. Mater. Sci.* **54**(3), 1741–1768 (2019)
52. A. Kunwar, H. Ma, H. Ma et al., On the increase of intermetallic compound's thickness at the cold side in liquid Sn and SnAg solders under thermal gradient[J]. *Mater. Lett.* **172**, 211–215 (2016)
53. D.T. Chu, Y.C. Chu, J.A. Lin et al., Growth competition between layer-type and porous-type Cu<sub>3</sub>Sn in micro-bumps[J]. *Microelectron. Reliab.* **79**, 32–37 (2017)
54. F.Y. Ouyang, Y.P. Su, Growth kinetic of Ag<sub>3</sub>Sn intermetallic compound in micro-scale Pb-free solder alloys under a temperature gradient[J]. *J. Alloy. Compd.* **655**, 155–164 (2016)
55. F.Y. Ouyang, G.L. Hong, Y.R. Hsu et al., Thermomigration in Co/SnAg/Co and Cu/SnAg/Co sandwich structure[J]. *Microelectron. Reliab.* **97**, 16–23 (2019)
56. Y.S. Yang, C.J. Yang, F.Y. Ouyang, Interfacial reaction of Ni<sub>3</sub>Sn<sub>4</sub> intermetallic compound in Ni/SnAg solder/Ni system under thermomigration[J]. *J. Alloy. Compd.* **674**, 331–340 (2016)
57. Y.S. Huang, H.Y. Hsiao, C. Chen et al., The effect of a concentration gradient on interfacial reactions in micro-bumps of Ni/SnAg/Cu during liquid-state soldering[J]. *Scripta Mater.* **66**(10), 741–744 (2012)
58. Y.W. Wang, Y.W. Lin, C.R. Kao, Kirkendall voids formation in the reaction between Ni-doped SnAg lead-free

- solders and different Cu substrates[J]. *Microelectron. Reliab.* **49**(3), 248–252 (2009)
59. J.G. Lee, K.N. Subramanian, Microstructural features contributing to enhanced behaviour of Sn-Ag based solder joints[J]. *Solder. Surf. Mount Technol.* **17**(1), 33–39 (2005)
  60. C.Y. Ho, M.T. Tsai, J.G. Duh et al., Bump height confinement governed solder alloy hardening in Cu/SnAg/Ni and Cu/SnAgCu/Ni joint assemblies[J]. *J. Alloy. Compd.* **600**, 199–203 (2014)
  61. H.R. Kotadia, O. Mokhtari, M. Bottrill et al., Reactions of Sn-3.5Ag-Based Solders Containing Zn and Al Additions on Cu and Ni(P) Substrates[J]. *J. Electron. Mater.* **39**(12), 2720–2731 (2010)
  62. M. Lu, D.Y. Shih, S.K. Kang et al., Effect of Zn doping on SnAg solder microstructure and electromigration stability[J]. *J. Appl. Phys.* **106**(5), 1611–1615 (2009)
  63. S. Tikale, K.N. Prabhu, Effect of multiple reflow cycles on the shear strength of nano-Al<sub>2</sub>O<sub>3</sub> particles reinforced Sn3.6Ag lead-free solder alloy[J]. *Trans. Indian Inst. Met.* **71**, 2855–2859 (2018)
  64. C. Yu, Y. Yang, K. Wang et al., Relation between Kirkendall voids and intermetallic compound layers in the SnAg/Cu solder joints[J]. *J. Mater. Sci.: Mater. Electron.* **23**(1), 124–129 (2012)
  65. C. Lee, C.Y. Lin, Y.W. Yen, The 260 °C phase equilibria of the Sn–Sb–Cu ternary system and interfacial reactions at the Sn–Sb/Cu joints[J]. *Intermetallics* **39**(35), 1027–1037 (2010)
  66. J.P. Curtulo, M. Dias, F. Bertelli et al., The application of an analytical model to solve an inverse heat conduction problem: Transient solidification of a Sn-Sb peritectic solder alloy on distinct substrates[J]. *J. Manuf. Process.* **48**, 164–173 (2019)
  67. X.N. Du, J.D. Guo, J.K. Shang, Effect of electromigration on interfacial reactions in 90Sn-10Sb Pb-free solder joints[J]. *J. Electron. Mater.* **38**(11), 2398–2404 (2009)
  68. C.H. Lee, W.T. Chen, C.N. Liao, Effect of antimony on vigorous interfacial reaction of Sn–Sb/Te couples[J]. *J. Alloy. Compd.* **509**(16), 5142–5146 (2011)
  69. B.Y. Han, F.L. Sun, T.H. Li et al., Microstructure evolution of Au/SnSb-CuNiAg/(Au)Ni during high temperature aging[J]. *Solder. Surf. Mount Technol.* **32**(2), 57–64 (2020)
  70. T.T. Dele-Afolabi, M. Hanim, M. Norkhairunnisa et al., Growth kinetics of intermetallic layer in lead-free Sn–5Sb solder reinforced with multi-walled carbon nanotubes[J]. *J. Mater. Sci.: Mater. Electron.* **26**(10), 8249–8259 (2015)
  71. N. Jiang, L. Zhang, Z.Q. Liu et al., Reliability issues of lead-free solder joints in electronic devices[J]. *Sci. Technol. Adv. Mater.* **20**(1), 876–901 (2019)
  72. B. Yeung, J.W. Jang, Correlation between mechanical tensile properties and microstructure of eutectic Sn-3.5Ag solder[J]. *J. Mater. Sci. Lett.* **21**(9), 723–726 (2002)
  73. W.M. Chen, P. McCloskey, S.C. O’Mathuna, Isothermal aging effects on the microstructure and solder bump shear strength of eutectic Sn37Pb and Sn3.5Ag solders[J]. *Microelectron. Reliab.* **46**(5–6), 896–904 (2006)
  74. H. Rhee, K.N. Subramanian, A. Lee et al., Mechanical characterization of Sn-3.5Ag solder joints at various temperatures[J]. *Solder. Surf. Mount Technol.* **15**(3), 21–26 (2003)
  75. M.Y. Guo, C.K. Lin, C. Chen et al., Asymmetrical growth of Cu<sub>6</sub>Sn<sub>5</sub> intermetallic compounds due to rapid thermomigration of Cu in molten SnAg solder joints - ScienceDirect[J]. *Intermetallics* **29**(10), 155–158 (2012)
  76. J. Keller, D. Baither, U. Wilke et al., Mechanical properties of Pb-free SnAg solder joints[J]. *Acta Mater.* **59**(7), 2731–2741 (2011)
  77. I. Shohji, T. Yoshida, T. Takahashi et al., Tensile properties of Sn-Ag based lead-free solders and strain rate sensitivity[J]. *Mater. Sci. Eng. A* **366**(1), 50–55 (2004)
  78. D.B. Witkin, Influence of microstructure on quasistatic and dynamic mechanical properties of bismuth-containing lead-free solder alloys-ScienceDirect[J]. *Mater. Sci. Eng., A* **532**(3), 212–220 (2012)
  79. P. Babaghorbani, S.M.L. Nai, M. Gupta, Development of lead-free Sn-3.5Ag/SnO<sub>2</sub> nanocomposite solders[J]. *J. Mater. Sci. Mater. Electron.* **20**(6), 571–576 (2009)
  80. P. Babaghorbani, S.M.L. Nai, M. Gupta, Reinforcements at nanometer length scale and the electrical resistivity of lead-free solders[J]. *J. Alloy. Compd.* **478**(1–2), 458–461 (2009)
  81. M. Lederer, A.B. Kotas, G. Khatibi, A lifetime assessment and prediction method for large area solder joints[J]. *Microelectron. Reliab.* **114**, 113888 (2020)
  82. M.J. Esfandyarpour, R. Mahmudi, Microstructure and tensile behavior of Sn–5Sb lead-free solder alloy containing Bi and Cu[J]. *Mater. Sci. Eng., A* **530**, 402–410 (2011)
  83. T.T. Dele-Afolabi, M.A. Azmah Hanim, M. Norkhairunnisa et al., Investigating the effect of isothermal aging on the morphology and shear strength of Sn-5Sb solder reinforced with carbon nanotubes[J]. *J. Alloy. Compd.* **649**, 368–374 (2015)
  84. A.R. Geranmayeh, R. Mahmudi, M. Kangooie, High-temperature shear strength of lead-free Sn–Sb–Ag/Al<sub>2</sub>O<sub>3</sub> composite solder[J]. *Mater. Sci. Eng., A* **528**(12), 3967–3972 (2011)
  85. O.L. Rocha, T.A. Costa, M. Dias et al., Cellular/dendritic transition, dendritic growth and microhardness in directionally solidified monophasic Sn-2%Sb alloy[J]. *Trans. Nonferr. Metal. Soc. China* **28**(8), 1686 (2018)



86. E.S. Gouda, E.M. Ahmed, F.A.S. Allah, Electrical and mechanical properties of Sn-5wt.% Sb alloy with annealing temperature[J]. *Eur. Phys. J. Appl. Phys.* **45**(1), 10901 (2009)
87. K.K. Xu, L. Zhang, L.L. Gao et al., Review of microstructure and properties of low temperature lead-free solder in electronic packaging[J]. *Sci. Technol. Adv. Mater.* **21**(1), 689–711 (2020)
88. Z. Xu, A. Sharma, S.J. Lee et al., Effect of soldering temperature on wetting and optical density of dip coated Sn and Sn-3.5Ag solders[J]. *Adv. Manuf. Process.* **30**(1), 127–132 (2015)
89. C.Y. Liu, L. Jian, G.J. Vandentop et al., Wetting reaction of Sn-Ag based solder systems on Cu substrates plated with Au and/or Pd layer[J]. *J. Electron. Mater.* **30**(5), 521–525 (2001)
90. V.U. Nayak, K.N. Prabhu, N. Stanford et al., Wetting behavior and evolution of microstructure of Sn-3.5Ag solder alloy on electroplated 304 stainless steel substrates[J]. *Trans. Indian Inst. Metal.* **65**(6), 713–717 (2012)
91. L.Y. Hsiao, J.G. Duh, Synthesis and characterization of lead-free solders with Sn-3.5Ag-xCu ( $x = 0.2, 0.5, 1.0$ ) alloy nanoparticles by the chemical reduction method[J]. *J. Electrochem. Soc.* **152**(9), J105–J109 (2005)
92. Peng L, Fu G. Effects of Ni particle addition on microstructure and properties of SnAg based composite solders[C]// *Electronics Packaging Technology Conference. IEEE, 2006.*
93. W. Min, X. Su, An investigation on surface tension of Sn-based lead free solders[J]. *J. Mater. Sci.: Mater. Electron.* **26**(11), 1–7 (2015)
94. M.M. El-Bahay, M. Mossalamy, M. Mahdy et al., Study of the mechanical and thermal properties of Sn-5 wt% Sb solder alloy at two annealing temperatures[J]. *Phys. Status Solidi* **198**(1), 76–90 (2003)
95. J.M. Song, Z.M. Wu, D.A. Huang, Two-stage nonequilibrium eutectic transformation in a Sn–3.5Ag–3In solder[J]. *Scr. Mater.* **56**, 413–416 (2007)
96. S.W. Chen, P.Y. Chen, C.H. Wang, Lowering of SnSb alloy melting points caused by substrate dissolution[J]. *J. Electron. Mater.* **35**(11), 1982–1985 (2006)
97. E.M.A. Ahmed, M.A. Amin, N. Tubaylah, Evolution of microstructure and physical properties of lead-free Sn–5Sb–Ag rapidly solidified solder alloys[J]. *Appl. Phys. A* **127**(6), 403 (2021)
98. E.S. Gouda, Effect of Solidification Conditions on Structure and Properties of Rapidly-Solidified Sn-7.5wt%Sb Alloy[J]. *Adv. Manuf. Process.* **22**(7–8), 842–845 (2007)
99. Q.K. Zhang, Z.F. Zhang, In situ observations on creep fatigue fracture behavior of Sn–4Ag/Cu solder joints[J]. *Acta Mater.* **59**(15), 6017–6028 (2011)
100. I. Dutta, C. Park, S. Choi, Impression creep characterization of rapidly cooled Sn–3.5Ag solders[J]. *Mater. Sci. Eng. A* **379**(1/2), 401–410 (2004)
101. D. Taneja, M. Volpert, F. Hodaj, Further insight into interfacial interactions in nickel/liquid Sn–Ag solder system at 230–350 °C[J]. *J. Mater. Sci.: Mater. Electron.* **28**(24), 1–13 (2017)
102. D. Witkin, Creep behavior of Bi-containing lead-free solder alloys[J]. *J. Electron. Mater.* **41**(2), 190–203 (2012)
103. Z.J. Yang, S.M. Yang, H.S. Yu et al., IMC and creep behavior in Lead-free solder joints of Sn-Ag and Sn-Ag-Cu alloy system by SP method[J]. *Int. J. Automot. Technol.* **15**(7), 1137–1142 (2014)
104. X. Huang, Z. Wang, Y. Yu, Thermomechanical properties and fatigue life evaluation of SnAgCu solder joints for microelectronic power module application[J]. *J. Market. Res.* **9**(3), 5533–5541 (2020)
105. F. Guo, J. Lee, K.N. Subramanian, Creep behaviour of composite lead-free electronic solder joints[J]. *Solder. Surf. Mount Technol.* **15**(1), 39–42 (2003)
106. L. Zhang, L. Sun, Y.H. Guo et al., Reliability of lead-free solder joints in CSP device under thermal cycling[J]. *J. Mater. Sci.: Mater. Electron.* **25**(3), 1209–1213 (2014)
107. M.D. Mathew, H. Yang, S. Movva et al., Creep deformation characteristics of tin and tin-based electronic solder alloys[J]. *Metall. and Mater. Trans. A.* **36**(1), 99–105 (2005)
108. R. Mahmudi, A. Maraghi, Shear punch creep behavior of cast lead-free solders[J]. *Mater. Sci. Eng. A* **599**, 180–185 (2014)
109. R. Mahmudi, A.R. Geranmayeh, M. Allami et al., Effect of homogenization on the indentation creep of cast lead-free Sn-5%Sb solder alloy[J]. *J. Electron. Mater.* **36**(12), 1703–1710 (2007)
110. A.R. Geranmayeh, R. Mahmudi, Power law indentation creep of Sn-5% Sb solder alloy[J]. *J. Mater. Sci.* **40**(13), 3361–3366 (2005)
111. R. Mahmudi, A.R. Geranmayeh, A. Rezaee-Bazzaz, Impression creep behavior of lead-free Sn–5Sb solder alloy[J]. *Mater. Sci. Eng., A* **448**(1–2), 287–293 (2007)
112. Y. Park, J.H. Bang, C.M. Oh et al., The effect of eutectic structure on the creep properties of Sn-3.0Ag-0.5Cu and Sn-8.0Sb-3.0Ag solders[J]. *Multidiscip. Digital Publish. Inst.* **7**(12), 540 (2017)
113. Z. Liang, S.B. Xue, L.L. Gao et al., Development of Sn–Zn lead-free solders bearing alloying elements[J]. *J. Mater. Mater. Electron.* **21**(1), 1–15 (2010)

114. S.L. Tay, A. Haseeb, M.R. Johan, Addition of cobalt nanoparticles into Sn-3.8Ag-0.7Cu lead-free solder by paste mixing[J]. *Solder. Surf. Mount Technol.* **23**(1), 10–14 (2011)

**Publisher's Note** Springer Nature remains neutral with regard to jurisdictional claims in published maps and institutional affiliations.